AD

41736

UNCLASSIFIED

THE MUNICIPAL UNIVERSITY OF WICHITA

AN EXPERIMENTAL COMPARISON OF CONSTANT-PRESSURE AND CONSTANT-DIAMETER JET PUMPS

by H.B. Helmbold, G. Luessen and A.M. Heinrich

Engineering Report No. 147

for the Office of Naval Research
Contract N-onr 201(01)

July 1954
University of Wichita
School of Engineering
Wichita, Kansas

AN EXPERIMENTAL COMPARISON OF CONSTANT-PRESSURE AND CONSTANT-DIAMETER JET PUMPS

by H.B. Helmbold, G. Luessen and A.M. Heinrich

Engineering Report No. 147

for the Office of Naval Research
Contract N-onr 201(01)

July 1954
University of Wichita
School of Engineering
Wichita, Kansas

AN EXPERIMENTAL COMPARISON OF CONSTANT-PRESSURE AND CONSTANT-DIAMETER JET PUMPS

SUMMARY

Two jet pumps, one of conventional constant-diameter design and the other of constant-pressure design (design initial-velocity ratio = 0.069), having identical jet-nozzle to mixing-tube area ratios and overall dimensions were compared for initial velocity ratios from 0.01 to 0.13.

With a constant static pressure gradient in its free-mixing section (initial-velocity ratio = 0.0755), the constant-pressure jet-pump efficiency was 20.3 percent, or 87.1 percent of the value theoretically predicted. This corresponded to a 31 percent improvement over the cylindrical jet pump efficiency which was 15.5 percent at the same initial velocity ratio ($a = 0.0755$). With the cylindrical jet pump, experimental efficiencies slightly greater than predicted by theory were obtained with the ring vortex present ($a < 0.0696$). Therefore the energy required to maintain a ring vortex was less than the energy conserved by mixing in the improved static pressure gradient which resulted from the vortex.

Good agreement between theoretical and experimental values was obtained for free-mixing-zone lengths and static pressures at the end of the free mixing zone for the cylindrical jet pump.

INTRODUCTION

As a result of the theoretical jet pump studies of references 1 to 4, the pumping performance of two types of mixing tubes - viz. cylindrical (constant diameter) and constant pressure - was compared. For simplicity it was assumed in the theory that the mixing fluids were identical and incompressible. In order to approximate these assumptions satisfactorily the jet Mach number was kept below .5 and the excess temperature of the jet was less than 10 percent of the absolute ambient temperature. Reference 1 shows that the constant pressure jet pump exhibits a greater theoretical efficiency than the constant diameter jet pump particularly at low initial velocity ratios. Therefore the design velocity ratio for the constant pressure jet pump was chosen in this region so that the superiority over the constant diameter jet pump could be clearly demonstrated.

NOMENCLATURE

SYMBOLS

$C_p = \frac{p_{t_3} - p_{t_1}}{q_3}$ net power or total pressure coefficient

f_I, f_Q form parameters of the excess velocity profile

$k = \dfrac{\left[\left(\frac{p_{t_3}}{p_0}\right)^{\frac{\gamma-1}{\gamma}} - 1\right]\frac{\rho_0}{\rho_3} - \left[\left(\frac{p_{t_1}}{p_0}\right)^{\frac{\gamma-1}{\gamma}} - 1\right]\frac{\rho_0}{\rho_1}}{\left(\frac{p_{t_0}}{p_0}\right)^{\frac{\gamma-1}{\gamma}} - 1 - \left[\left(\frac{p_{t_1}}{p_0}\right)^{\frac{\gamma-1}{\gamma}} - 1\right]\frac{\rho_0}{\rho_1}}$ experimental transmission coefficient

k_{th} theoretical transmission coefficient

$k_{th} = \frac{1 + (1+2\mu)\alpha}{(1+\mu)^2(1+\alpha)}$ with constant pressure

$k_{th} = \frac{\beta^2 - \alpha}{1-\alpha}$ with constant diameter

K kinematic momentum flux

L length of the free mixing zone

M_0 jet Mach number at nozzle exit

p static pressure

p_t total pressure

q $\frac{1}{2}\rho u^2$ dynamic pressure

Q volume flux or quantity flow

r_o nozzle exit radius

r_1 mixing tube radius at initial plane

$r_{1/2}$ radius where the local velocity is one-half the maximum velocity at a cross section (with the jet in still air)

$r_{\sqrt{1/2}}$ radius where the total pressure is one-half the maximum total pressure at a cross section (with the jet in still air)

R radius of constant diameter tube (equal to R_2 for constant pressure mixing tube)

S cross sectional area

u velocity

U_a velocity at the tube wall

ΔU Maximum excess velocity

x axial coordinate

y outer radius of free mixing zone

$\alpha = u_1/u_0$ initial velocity ratio

$\beta = u_2/u_0$ final velocity ratio at test (final) plane

γ ratio of specific heats, constant volume/constant pressure

κ_{III} non-dimensional coefficient defined by the axial slope of the outer radii of the mixing zone in still air (See ref. 3)

κ_{IV} empirical diffusion constant (See ref. 4)

η $(1+\mu)k$ experimental efficiency

$\eta_i = (1+\mu)k_{th}$ ideal efficiency

ρ density

$\phi = S_0/S_1 = \dfrac{r_0^2}{r_1^2 - r_0^2}$ area ratio at initial plane

$\mu = \dfrac{S_1 u_1 \rho_1}{S_0 u_0 \rho_0} = \dfrac{\rho_1 \alpha}{\rho_0 \phi}$ = mass ratio, induced flow/jet flow

Subscripts

0 jet flow at nozzle exit (initial plane)

1 secondary flow at initial plane

2 mixture at final plane (test plane)

3 mixture transformed from state at final plane to a perfect mixture occuring theoretically at some distance far downstream.

∞ ambient air

$\bar{}$ (bar) denotes mixed flow brought back to initial static pressure, p_1

$*$ denotes value at the end of the free mixing zone, i.e. beginning of the guided mixing zone.

EXPERIMENTAL METHOD

Apparatus

The experimental jet pump consisted of a compressor that supplied primary flow through a convergent nozzle, and the pump body that included an entrance cone, interchangeable mixing tubes, and an exit diffuser. (figs. 1 and 2)

The 3 stage centrifugal compressor was belt driven at a speed ratio of 3:1 by a 7.5 HP, 3 phase, 1750 RPM, squirrel-cage induction motor. With a jet exit area of 0.279 square inches (r_o = 0.298 in.) the compressor had sufficient capacity for a jet Mach number, M_o, of approximately 0.6.

The entrance bell mouth and jet nozzle contours were designed by the method of reference 9. The original nozzle design was unsatisfactory because flow separation occurred on its exterior tapered portion. An attempt to correct this condition by fairing a transition from the cylindrical pipe to the conical portion of the nozzle was unsuccessful. Therefore a lengthened nozzle with an improved external contour (see figure 3) was designed and the inside diameter of the duct pipe was reduced from 2 inches to 1-1/2 inches. Although separation did not occur with the modified nozzle, some sacrifice was made in the rectangularity of the jet velocity profile because the increased length produced a thicker boundary layer in the primary air stream.

The jet temperature was not controlled. However, at no time did the temperature differential between primary and secondary flows exceed 10 percent of the secondary air temperature. The nozzle exit was located at station 3 for all tests.

Two mixing tubes were tested - viz. a conventional constant diameter tube and a constant pressure tube (design α = 0.069, C_p = 5.0). In order to make a fair comparison of the two jet pumps it was necessary that they have the same overall dimensions - i.e. identical initial radii, exit radii = R_2 = 3 inches, and lengths = 19 R_2 = 57 inches - as well as equal initial velocity ratios. In order to compensate for the presence of the nozzle and maintain the design area ratio (ϕ = .01) the radii at the initial plane were enlarged to 3.015 inches.

The constant pressure mixing tube was designed by methods described in references 3 and 4 (table I shows the basic dimensions). Since a constant pressure free mixing zone requires a wall contraction it was necessary to fair the constant pressure mixing section into a diffuser for R_2 to be the required 3 inches (schematic figure 5). At the end of this diffuser was a straightening section 6 inches long to provide parallel flow in the final plane. For a similar reason both jet pumps were provided with a straightening section extending 3 inches upstream from the initial plane.

A conical valve with a screw adjustment was used to control the initial velocity ratio.

Glass cloth impregnated with a thermosetting casting resin (Renite) was used in fabrication of the entrance section, mixing tubes and exit diffuser.

Instrumentation and Calibration

Static pressure taps having orifices of 1/32 inch diameter were located at 3 inch intervals downstream of station 3.75 plus one each at the initial plane, station 3.00, and the final plane, station 60.00. Since the assumption was made that a constant static pressure existed across each cross section, the static pressures were measured only at the mixing tube walls.

Every other static pressure tap was screw threaded (figure 4) so that the total pressure probe could be inserted in its place. At these stations total pressure probe fittings were also provided 90° radially to permit normal diametral surveys. The tip of the total pressure probe was .032 inch outside diameter tubing to permit total pressure measurements near the mixing tube wall. Radial positions could be set to .01 inch by the attached scale.

A rake consisting of 21 total pressure tubes mounted on a crossbar was located at the final plane. These total-pressure tubes and the static pressure taps were connected to a multiple-tube manometer for photographically recording the data. The rake showed the flow to be unsteady at high initial-velocity ratios, hence data were taken only when the maximum total pressure was at the mixing tube centerline.

Since the loss of total pressure of the entrance section was negligible and the initial-plane velocity distribution was very nearly constant, u_1 was determined from the gage static pressure at the wall of the initial plane, or q_1. Both q_1 and the total pressure surveys away from the high total pressures of the jet were measured on a micromanometer.

Calibration of the jet nozzle in still air for various u_o (actually an average u_o over the jet) was performed by making radial total pressure surveys at the nozzle exit with different compressor intake valve settings. Static pressure across the jet at the nozzle exit was assumed ambient. Conventional compressible flow relations were used in data reduction. The jet temperature was measured upstream of the nozzle where low velocities made recovery factor corrections unnecessary.

TESTS

Longitudinal static pressure distributions and total pressure surveys at the final plane were made in α increments of approximately 0.01 up to a maximum of 0.13 for both the constant-diameter and constant-pressure mixing tubes. The velocity ratio was adjusted by means of the conical valve at the end of the exit diffuser. In addition to these data required for performance evaluation, diametral total pressure surveys were taken at initial velocity ratios of 0.02 (showing the ring vortex) and 0.08 for the constant diameter mixing tube, and at the design α of 0.069 for the constant-pressure mixing tube.

A systematic investigation was conducted to determine the α at which the ring vortex originated for the constant diameter mixing tube. The presence of the ring vortex was confirmed for the constant pressure mixing tube at an α of 0.02. Reverse flow was determined by noting a decreasing rather than increasing tendency in the measured values of total pressure as the probe was moved away from the mixing tube wall. The probe was pointed in the normal upstream direction at all times.

Surveys were made of the jet in free air to measure the jet spreading coefficient and thereby check the value assumed in the constant pressure mixing tube design. This was done for both the original and the modified nozzle. Data were taken at distances up to 80 nozzle diameters from the jet exit for the original nozzle and up to 35 diameters for the modified nozzle.

RESULTS AND DISCUSSION

Efficiencies

The prime purpose of these jet pump experiments was to show the economical superiority of the jet mixing process at constant static pressure (or with axially decreasing pressure) over that for axially increasing pressure which occurs in the conventional constant-diameter jet pump. As

shown in reference 1 and stated in reference 7, the economical superiority of a constant pressure or decreasing pressure mixing tube is easily understood. The energy lost in the mixing process is the work done by the turbulent shearing stresses. This work can be reduced by decreasing the velocity differential between the primary and the secondary flows. A positive pressure gradient, as in the cylindrical mixing tube, decreases the velocity of the weaker secondary flow more in proportion than the velocity of the stronger jet causing an adverse effect on this velocity difference. Conversely, a negative pressure gradient supports the equalizing effect of the mixing process and so reduces the work done by the turbulent shearing stresses.

The ideal efficiency of the constant-pressure jet pump (at its design condition) is always greater than for the cylindrical tube. However, at high velocity ratios the small gain in ideal efficiency is more than lost in the diffuser of an actual pump. Therefore the superiority of constant-pressure jet pumps is limited in velocity ratio. The design conditions for the constant-pressure mixing tube in this experiment were chosen in the low velocity ratio region so that the superiority over the constant diameter mixing tube could be clearly demonstrated.

An efficiency of the perfect mixing process, i.e. that mixing process completed theoretically only at some distance far downstream where the total pressure would be constant across the cross section, was defined by considering the transmission of jet kinetic energy to the secondary flow with the final static pressure equal to initial static pressure. This meant that for performance evaluation the experimental flow as measured at the test plane was first transformed without losses to a perfectly mixed state and then isentropically expanded back to the initial static pressure. The relations used in this procedure were the following:

$$\eta = (1+\mu)k$$

with

$$k = \frac{\left[\left(\frac{p_{t_2}}{p_0}\right)^{\frac{\gamma-1}{\gamma}} - 1\right]\frac{\rho_0}{\rho_3} - \left[\left(\frac{p_{t_1}}{p_0}\right)^{\frac{\gamma-1}{\gamma}} - 1\right]\frac{\rho_0}{\rho_1}}{\left(\frac{p_{t_0}}{p_0}\right)^{\frac{\gamma-1}{\gamma}} - 1 - \left[\left(\frac{p_{t_1}}{p_0}\right)^{\frac{\gamma-1}{\gamma}} - 1\right]\frac{\rho_0}{\rho_1}} \quad \text{(See ref. 6)}$$

The density ratio $(\frac{\rho_0}{\rho_3})$ was calculated

for <u>constant pressure</u> by

$$\frac{\rho_0}{\rho_3} = \frac{1 + \frac{\rho_0}{\rho_1}\mu}{1+\mu} + \frac{\gamma-1}{2}(M_0^2)\frac{\mu}{(1+\mu)^2}(1-\alpha)^2$$

and for <u>constant diameter</u> by

$$\frac{\rho_0}{\rho_3} = \frac{\rho_0}{\rho_3}\left(\frac{p_3}{p_0}\right)^{\frac{1}{\gamma}} \quad \text{(See ref. 6)}$$

The <u>ideal efficiency</u> used was

$$\eta_i = (1+\mu)k_{th}.$$

The theoretical values of the transmission coefficient were defined as

$$k_{th} = \frac{1 + (1+2\mu)\alpha}{(1+\mu)^2(1+\alpha)} \quad \text{for } \underline{\text{constant pressure}}$$

and

$$k_{th} = \frac{\bar{\beta}^2 - \alpha}{1-\alpha} \quad \text{for } \underline{\text{constant diameter}}, \text{ where } \bar{\beta}^2 \text{ is}$$

the final velocity ratio at some distance far downstream and was found approximately from

$$\bar{\beta}^2 \approx \left[2\left(\frac{1+\mu\alpha}{1+\mu}\right) - \beta\right]\beta$$

with

$$\beta \approx \frac{\frac{S_2}{S_0} + \gamma M_0^2 (1+\mu\alpha)}{1 + \mu\frac{\rho_0}{\rho_1} + \frac{\gamma-1}{2}M_0^2(1+\mu\alpha^2)} \quad \text{(See ref. 6)}$$

In these calculations the ratio $\frac{\rho_1}{\rho_0}$ was assumed to be an average of test values (see tables II and III). Boundary layer losses were neglected in the ideal efficiency evaluation. It is important to understand that the curve of ideal efficiency for the constant-pressure mixing (fig. 6) actually represents a family of constant pressure jet pumps each designed for a given area ratio, ϕ, and various initial velocity ratios.

The experimental efficiency of the constant pressure jet pump was 20.3 percent, or 87.1 percent of the ideal efficiency when the static pressure was approximately constant in the free mixing zone, i.e. at the initial-velocity ratio equal to 0.0755 (fig. 6). Figure 11 shows the region of nearly zero axial static pressure gradient at $\alpha = 0.0755$. Constant pressure in the mixing section did not occur at the design $\alpha(\alpha = 0.069)$, because the actual jet spreading coefficient was larger than that assumed in the design of the mixing tube (discussed more fully in the Appendix I on jet spreading coefficient).

The difference between ideal and experimental efficiencies on the constant pressure jet pump resulted for two reasons: (1) the mixing process was not completed in the constant pressure section of the mixing tube, but continued in the diffuser under an adverse pressure gradient, and (2) friction losses occurred throughout the pump. With velocity ratios less than 0.0755 the mixing losses increased because the mixing was performed under adverse (positive) static pressure gradients, and at very low velocity ratios the presence of a ring vortex caused additional energy losses (these were partially overcome by mixing in the improved static pressure gradient, see figures 11 and 12 for $\alpha \leq 0.03$) Existence of the ring vortex was verified at $\alpha = 0.02$. For velocity ratios greater than 0.0755 the diffuser losses increased, whereas mixing losses were diminished by favorable pressure gradients in the mixing tube. As the velocity ratio was increased the diffuser losses eventually outweighed gains obtained by mixing under decreasing static pressure gradients and the efficiency decreased (see figure 6).

The losses other than mixing losses in the constant-diameter mixing tube were essentially in the boundary layer and therefore were appreciable only at high velocity ratios. It was predicted (reference 2) that reverse flow would occur in the cylindrical mixing tube for total-pressure coefficients, C_p, greater than 4.556. This numerical value depended entirely on the shape of the excess velocity profile at the end of the free mixing zone which was not very well known when the prediction was made. An evaluation of the experimental excess velocity profile at station 18.00 with $\alpha = 0.08$ suggested that a more correct theoretical value of critical total-pressure coefficient would have been $C_p = 3.44$, if the presence of the boundary layer at the wall was neglected.

The systematic investigation of total pressures along the wall of the constant diameter jet pump revealed that reverse flow did occur for all initial-velocity ratios less than 0.0696, i.e. C_p values greater than 2.76. The difference between the revised theoretical and the experimental values can be explained by the presence of the boundary layer at the wall, which in an adverse pressure gradient is always more prone to reverse flow direction than the secondary-air potential flow with its higher kinetic energy (in potential flow reversal originates when the increase of static pressure from the initial plane to the end of the free mixing zone equals the initial dynamic pressure of the secondary flow). Before the tests, conjectures were made as to whether mixing gains due to suppression of the adverse static pressure gradient by the ring vortex (figures 13 and 14) would offset the additional energy required to form the vortex. This was actually the case as shown by the fact that experimental efficiencies were slightly above the theoretical values on the constant diameter jet pump for a less than 0.07.

The superiority of the constant-pressure jet pump over the constant-diameter jet pump was evident over a wide range of working conditions (figure 6). With constant pressure in the constant pressure mixing tube ($a = 0.075$) the improvement amounted to 31 percent of the constant diameter jet pump efficiency which was 15.5 percent at that a. Figure 7 shows the range of mass ratios for the tests. Since the transmission coefficient, k, is the ratio of the specific kinetic energies of the perfectly mixed flow (at $p = p_1$) to the primary flow, the graph of figure 8 shows in another fashion the increasing superiority of the constant pressure design at low velocity ratios. A further comparison of the two mixing tubes is shown by the static pressure plots (figures 9 and 10). Since the dynamic pressures at the final plane were approximately equal for a given a, the greater increase in static pressure indicated more efficient mixing.

Length of the Free Mixing Zone in the Cylindrical Mixing Tube

The length of the free mixing zone from a point orifice in a cylindrical mixing tube was theoretically predicted from the following table (ref. 3):

C_p	$16\, k_{TTT} \frac{L}{D}$
0.2	2.605
0.5	1.694
1.0	1.3[illegible]
2.0	1.1[illegible]
4.556	1.000

where the total pressure coefficient was defined as $C_p \equiv \frac{p_{t_3} - p_{t_1}}{q_3}$. The non-dimensional coefficient κ_{III} was defined by the axial slope of the outer radii, y, of the mixing zone in <u>still air</u> - i.e.

$$\frac{dy}{dx} = 16\ \kappa_{III}$$

The slope $\frac{dy}{dx}$ can be determined from $\frac{dr_{\sqrt{1/2}}}{dx}$ (Reichardt's value 0.060, reference 10) and the constant ratio $\frac{r_{\sqrt{1/2}}}{y}$. Since $\frac{r_{\sqrt{1/2}}}{y} = 0.232$ (ref. 11), then $\frac{dy}{dx} = \frac{0.060}{0.232} = 0.2586 = 16\kappa_{III}$. The lengths of the free mixing zones in the constant-diameter tube were calculated using the numerical factor $16\kappa_{III} = 0.2586$, and are denoted as dashed curves in figures 13 and 14. In agreement with Reichardt's results it was assumed that the equivalent point orifice was located at the initial plane . These curves came close to the locus of the first inflection points of the axial pressure distributions (for those velocity ratios where no ring vortex occurs, namely $\alpha > 0.0696$). Theoretical considerations on the connection between pressure distribution and excess velocity profile led to the conclusion that the first inflection points defined the actual end of the free mixing zone if reverse flow did not exist. The presence of reverse flow in the mixing zone was indicated on the axial pressure distributions by a flat portion at low velocity ratios and a dip at smallest velocity ratios (figures 11 to 14). The dip for α less than 0.03 (on either mixing tube) was explained as a thickening of the ring vortex as α decreased, causing radial velocities that lowered the local static pressure.

Similarity of Static-Pressure Distributions in the Guided Mixing Zone of the Cylindrical Mixing Tube

Empirically the static-pressure distributions in the guided mixing zone can be reduced to a single curve,

$$\frac{\sqrt{p_2 - p}}{q_2} = f\left[C_p \left(\frac{x}{R} - 7.21 - \frac{6.80}{\sqrt{C_p}}\right)\right]$$

at least for a wide range of total pressure coefficients as shown by figure 15. The greater part of these curves were straight lines. These statements are not applicable

to the higher total-pressure coefficients when a strong ring vortex was formed in the mixing tube nor to the lowest total-pressure coefficient when the flow had large fluctuations. The reduced curves, however, were wholly or at least partially straight lines with slopes not much different from those of medium total-pressure coefficients.

Total Pressure Surveys

The total-pressure surveys (figs. 16 through 34) show the progression of the free mixing zone toward the wall of the mixing tube and the change in the type of velocity profile from the free mixing zone to the guided mixing zone. The series on the cylindrical mixing tube at an a of 0.02 (figures 29 to 34) shows the boundary of the ring vortex. It should be stated that the total pressure values on these surveys are averages taken over a period of several minutes. Due to the irregular, low-frequency pressure variations of large amplitude which were superimposed on higher-frequencyed, small amplitude pressure variations averaged values were deemed most representative. Other investigators - viz. Viktorin - also reported similar difficulties in making readings.

Since the total pressure probe always faced upstream, those values in the region of reverse flow have no physical significance other than to indicate the presence of reverse flow. This is the reason that these values are connected by a dotted curve on the plots.

CONCLUSIONS

At low velocity ratios where the ideal efficiencies of the constant pressure jet pumps are considerably greater than for the constant diameter jet pumps, the incorporation of constant pressure design improved performance to a great extent. Moreover, a constant pressure pump designed to operate at a low velocity ratio will exhibit its superiority over a wide range of working conditions.

Large diffuser losses which occurred at high velocity ratios nullified gains of mixing economy secured by favorable static pressure gradients in the constant pressure jet pump. Therefore, if the restriction imposed by the test (that the overall dimensions for the constant pressure and cylindrical jet pumps must be equal) were revoked so that the diffuser on the constant-pressure jet pump would be unnecessary, the experimental efficiencies for this pump would have been much nearer to those predicted by theory.

The presence of the ring vortex in the mixing tube suppressed an adverse (increasing) static pressure gradient. It was found that the energy required to maintain such a ring vortex in the cylindrical jet pump was less than the energy saved by mixing in a more favorable static-pressure gradient. The result was an experimental efficiency slightly greater than that predicted by theory for the cylindrical jet pump.

A similarity of static pressure distributions existed in the guided mixing zone of the cylindrical mixing tube when the velocity ratio was neither low enough to have a ring vortex nor excessively high as to have large pressure fluctuations. A theoretical explanation for the observed similarity was not found.

REFERENCES

1.- Helmbold, H.B.: Contributions to the Jet Pump Theory I, Comparison of Ideal Mixing Processes. University of Wichita Engineering Study No. 105, June 1953.

2.- Helmbold, H.B.: Contributions to the Jet Pump Theory II, Integral Relations on Mixing Processes. University of Wichita Engineering Study No. 106, June 1953.

3.- Helmbold, H.B.: Contributions to the Jet Pump Theory III, Simplified Theory of Mixing Zone Spreading. University of Wichita Engineering Study No. 107, July 1953.

4.- Helmbold, H.B.: Contributions to the Jet Pump Theory IV, Approximate Theory of Jet Diffusion in a Constant Pressure Mixing Tube. University of Wichita Engineering Study No. 118, November 1953.

5.- Helmbold, H.B.: Contributions to Jet Pump Theory V, Simplified Theory of the Plane Jet in a Parallel Stream Under Constant Pressure, University of Wichita Engineering Study No. 137, May 1954.

6.- Helmbold, H.B.: Contributions to Jet Pump Theory VI, Perfect Mixing Processes in Subsonic Jet Pumps. University of Wichita Engineering Study No. 145, June 1954.

7.- Helmbold, H.B.: Review of a Systematic, Theoretical Investigation of Jet Pumps. University of Wichita Engineering Study No. 122, November 1953.

8.- Helmbold, H.B.; and Wallace, Richard E.: Pre-Test Report for a Systematic Investigation of Constant-Diameter and Constant-Pressure Jet Pumps. University of Wichita Engineering Study No. 121, November 1953.

9.- Tsien, Hsue-Shen: On the Design of a Contraction Cone for a Wind Tunnel. J.A.S., February 1943.

10.- Reichardt, H.: Gesetzmäszigkeiten der freien Turbulenz. VDI-Forschungsheft No. 414, Second Edition 1951.

11.- Tollmien, W.: Calculation of Turbulent Expansion Processes (1926). NACA-TM No. 1085, September 1945.

12.- Schlichting, H.: Grenzschichttheorie. Karlsruhe 1951.

APPENDIX I

JET SPREADING COEFFICIENT

Measurement of the jet spreading coefficient in still air was made for two reasons: (1) because of the range of spreading coefficient values given in literature, and (2) for a check on the value assumed in the design of the constant-pressure mixing tube.

Tollmien's value for the slope of $r_{1/2}$ plotted versus distance from the nozzle (i.e., spreading coefficient) is 0.077, but this value proved somewhat low because the measurements were not taken sufficiently far downstream from the nozzle. A British investigation at R.A.E. yielded a spreading coefficient of 0.0875 which was near Reichardt's value. Reichardt reported a slope of $r_{\sqrt{1/2}}$ versus distance from the nozzle equal to 0.060. If this value is transformed into spreading coefficient form by the constant ratios

$$\frac{r_{\sqrt{1/2}}}{y} = 0.232 \qquad \text{and} \qquad \frac{r_{1/2}}{y} = 0.36$$

according to the theoretical velocity distribution calculated by Tollmien (reference 11), the result is

$$\frac{dr_{1/2}}{dx} = \frac{0.06(0.36)}{0.232} = 0.0931$$

With low temperature differences between the jet and the surrounding air, the present tests yielded

$$\frac{dr_{1/2}}{dx} = 0.0928. \quad \text{(Fig. 35)}$$

The shifting of the curve of half-maximum velocity radii upward in the case of the modified nozzle (fig. 35) was probably due to the thicker boundary layer in that nozzle caused by its elongation (fig. 4). A density correction based on the temperature differential was tried, but the correction was found to be less than the experimental scatter.

Schlicting (reference 12) overlooked that Reichardt refers to the radius of half maximum total pressure, $r_{\sqrt{1/2}}$, instead of the more commonly used half maximum velocity radius, $r_{1/2}$. Consequently the following corrections to reference 4 must be stated.

(1) $r_{1/2} = 0.0931x$ instead of equation IV83 stating $r_{1/2} = 0.06x$.

(2) $y = 0.2586x$ instead of equation IV85

(3) $\kappa_{IV}^2 = 0.0068$ or

$\kappa_{IV} = 0.0825$ instead of equation IV87.

Since the smaller jet spreading coefficient was assumed in the design of the constant pressure mixing tubes (equation IV83), the need for the initial velocity ratio, α, to be 0.0755 instead of the design value of 0.069 for constant pressure in the free mixing zone is explained at least in a qualitative manner.

APPENDIX II

STATIC PRESSURE AT THE END OF THE FREE MIXING ZONE IN THE CYLINDRICAL MIXING TUBE

At the end of the free mixing zone and in the guided mixing zone, the radius of the mixing zone, y, is identical with the constant radius of the cylindrical mixing tube, R. Since the volume flux, Q, is constant, the velocity

$$\frac{Q}{\pi R^2} = U_a + f_Q \cdot \Delta U = u_3$$

is a constant too. Here U_a denotes the velocity at the tube wall and ΔU the maximum excess velocity; f_Q is a form parameter of the excess-velocity profile. These quantities are functions of the axial coordinate, x.

Dividing the kinematic momentum flux, K, by the cross-sectional area gives

$$\frac{K}{\pi R^2} = U_a^2 + 2f_Q U_a \Delta U + f_I \Delta U^2$$

which specializes at some distance far downstream to

$$\frac{K_3}{\pi R^2} = u_3^2.$$

The momentum theorem states that

$$p_3 - p = \rho \frac{K - K_3}{\pi R^2} = \rho(U_a^2 + 2f_Q U_a \Delta U + f_I \Delta U^2 - u_3^2).$$

By substituting

$$U_a = u_3 - f_Q \cdot \Delta U$$

The result is

$$p_3 - p = (f_I - f_Q^2)\, \rho \cdot \Delta U^2$$

or

$$\sqrt{\frac{p_3 - p}{q_3}} = \sqrt{2(f_I - f_Q^2)}\ \frac{\Delta U}{u_3}$$

Where $q_3 \equiv \rho u_3^2/2$. In ref. 3 it was assumed that in the free mixing zone $f_Q = \frac{1}{5}$ and $f_I = \frac{1}{9}$ (eqs. III 8b). On this basis the equation III 13 (ref. 3) was derived which specialized at the end of the free mixing zone to

$$\frac{\Delta U^*}{u_3} = \frac{15}{23}\left(-3 + \sqrt{1+23C_p}\right)$$

Substituting for $\Delta U^*/u_3$ and $\sqrt{2(f_I - f_{\xi})} = 0.3772$ yields

$$\frac{\sqrt{p_3 - p^*}}{q_3} = 0.738\left(-1 + \sqrt{1 + 2.556\ C_p}\right)$$

where p^* denotes the static pressure at the end of the free mixing zone, i.e. at the start of the guided mixing zone. The asymptotic pressure, p_3, can be equated to the pressure p_2 in the exit plane if this plane is situated sufficiently far downstream as in these experiments. However, the presence of the rake in the flow altered the static pressure reading in the final plane as can be seen on the static pressure plots, and p_2 was read at the next static pressure tap upstream from the final plane. Values of q_2 were also based on the same static pressure readings. The theoretical function is compared with the experimental results in figure 36. The experimental values of p^* were read from the pressure distribution plots, figures 13 and 14, at the first inflection points.

TABLE I MIXING TUBE DIAMETERS

CONSTANT PRESSURE MIXING TUBE (α DESIGN = .069)

Axial Distance From Initial Plane (Inches)	Diameter (Inches)
.000	6.000
1.245	5.850
2.895	5.670
4.689	5.484
6.591	5.301
8.637	5.118
10.785	4.932
13.095	4.746
15.540	4.560
17.100	4.446
20.100	4.262
21.100	4.141
26.100	4.082
29.100	4.085
32.100	4.151
35.100	4.279
38.100	4.470
41.100	4.723
44.100	5.038
47.100	5.415
50.100	5.855
51.000	6.000

TABLE II NUMERICAL RESULTS FOR CONSTANT PRESSURE JET PUMP

α	M_o	$\frac{p_{t_o}}{p_o}$	$\frac{p_{t_1}}{p_o}$	$\frac{p_{t_3}}{p_o}$	$\frac{\rho_o}{\rho_1}$	$\frac{\rho_o}{\rho_3}$	μ	k	η	η_1
.0131	.474	1.1655	1.000029	1.005115	.925	.966	1.44	.03140	.0766	.425
.02	.469	1.1656	1.000069	1.00503	.912	.948	2.22	.03005	.0968	.3385
.03	.473	1.1657	1.000154	1.004945	.916	.941	3.32	.02880	.1244	.276
.0406	.469	1.1681	1.000283	1.004845	.911	.934	4.46	.02686	.1469	.248
.05	.469	1.1660	1.000426	1.00481	.916	.932	5.54	.02595	.1695	.2335
.06	.469	1.1665	1.000615	1.004705	.916	.931	6.63	.02438	.1860	.2295
.069	.469	1.1667	1.000810	1.004625	.911	.927	7.68	.02262	.1963	.230
.08	.469	1.1680	1.001094	1.00460	.920	.930	8.81	.02085	.2045	.236
.09	.469	1.1687	1.001381	1.00461	.920	.929	9.91	.01934	.2111	.242
.095	.469	1.1666	1.001544	1.004595	.916	.926	10.52	.01847	.2128	.246
.10	.472	1.1697	1.001735	1.00465	.920	.930	11.01	.01762	.2116	.250
.11	.472	1.1701	1.002112	1.00469	.920	.930	12.13	.01568	.2059	.259
.12	.473	1.1707	1.002514	1.00476	.920	.928	13.22	.01373	.1953	.267

TABLE III NUMERICAL RESULTS FOR CONSTANT DIAMETER JET PUMP

α	M_o	$\frac{Pt_o}{P_o}$	$\frac{Pt_1}{P_o}$	$\frac{Pt_3}{P_o}$	$\frac{\rho_o}{\rho_1}$	$\frac{\rho_o}{\rho_3}$	μ	k	η	η_1
.02	.474	1.1660	1.000069	1.003203	.928	.969	2.18	.01933	.0615	.0584
.0274	.469	1.1672	1.000128	1.003205	.924	.956	3.01	.01866	.0748	.073
.03	.469	1.1668	1.000152	1.003215	.925	.954	3.28	.01860	.0796	.077
.04	.470	1.1673	1.000275	1.00325	.921	.945	4.40	.01784	.0963	.095
.05	.470	1.1674	1.000426	1.003335	.924	.942	5.50	.01740	.1131	.113
.06	.470	1.1668	1.000612	1.00347	.919	.938	6.62	.01741	.1327	.130
.07	.470	1.1675	1.000833	1.00362	.924	.942	7.69	.01682	.1462	.147
.08	.470	1.1678	1.001090	1.003815	.924	.938	8.79	.01638	.1603	.164
.09	.469	1.1681	1.001386	1.00404	.919	.933	9.91	.01596	.1741	.181
.10	.467	1.1674	1.001687	1.00425	.925	.940	10.94	.01567	.1870	.197
.11	.467	1.1674	1.002032	1.00449	.924	.937	12.01	.01501	.1952	.214
.12	.464	1.1678	1.002406	1.00479	.930	.944	13.04	.01464	.2056	.229
.13	.464	1.1678	1.002820	1.00515	.928	.943	14.16	.01444	.2189	.245

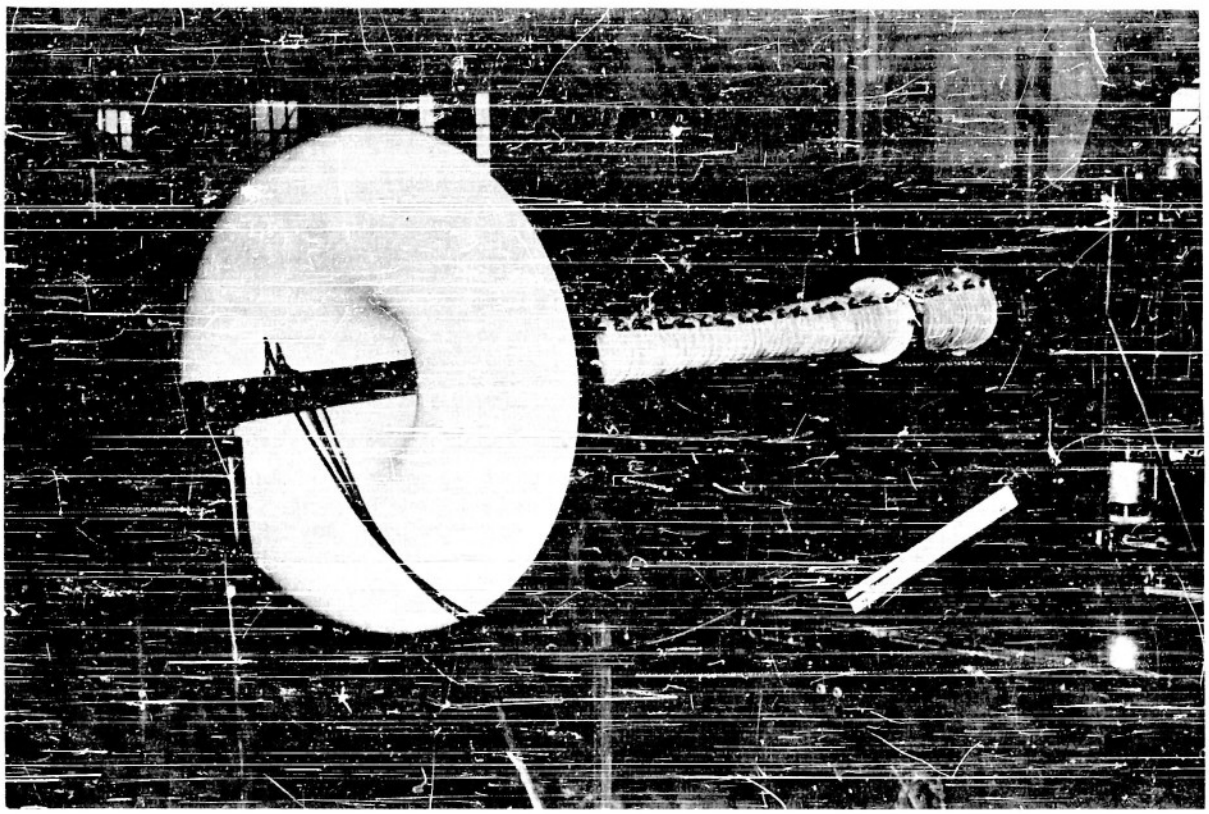

Figure 1.- Jet pump apparatus with C-P mixing tube installed

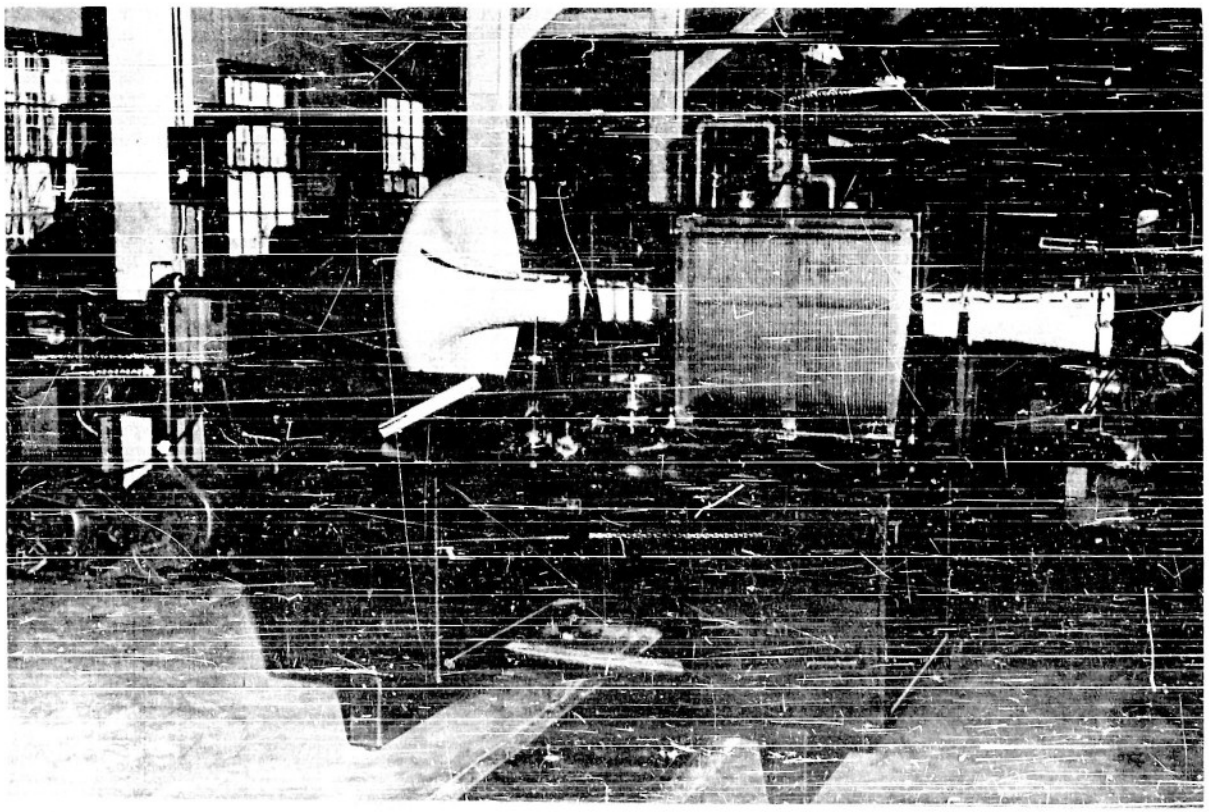

Figure 2.- Jet pump test setup showing the compressor

Figure 3.- Original and modified (lengthened) nozzles

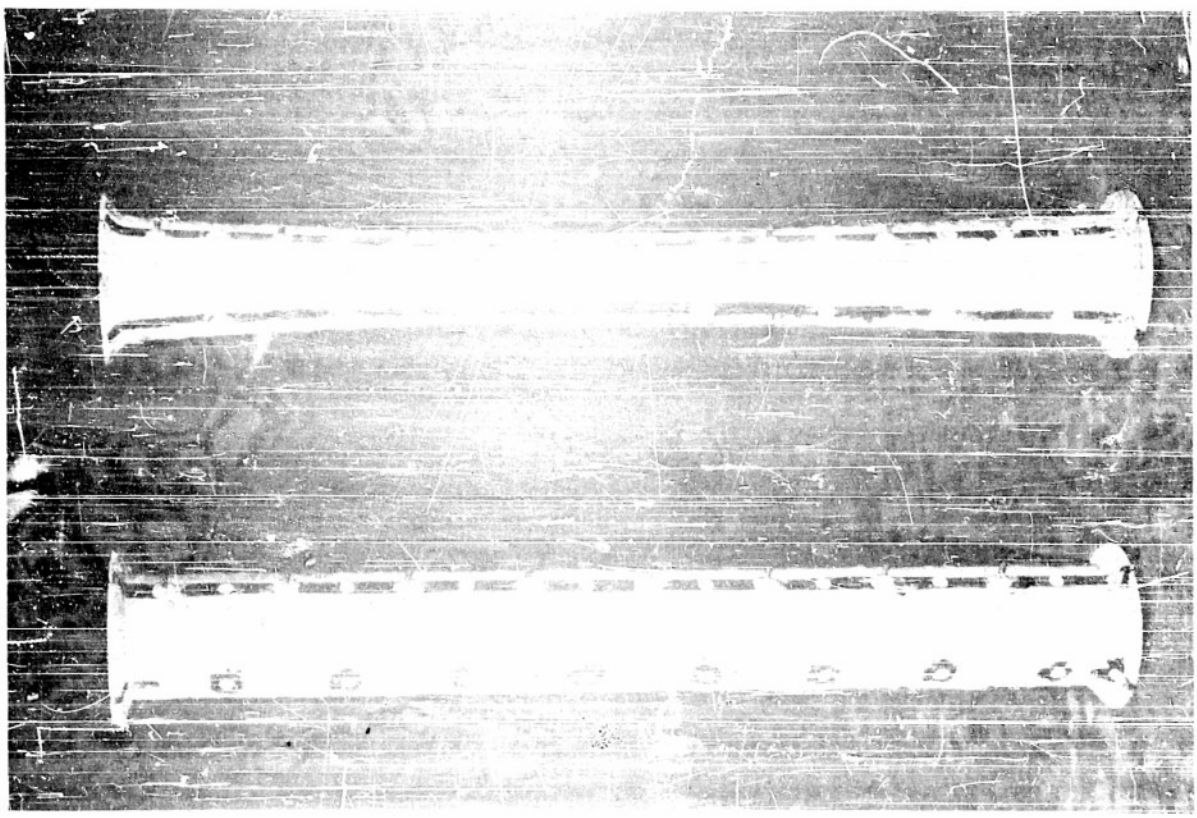

Figure 4.- Constant-pressure and constant-diameter mixing tubes

UNIVERSITY OF WICHITA
SCHOOL OF ENGINEERING

SCALES
DIMENSIONS 1/5 FULL SIZE
VELOCITY PROFILES 1 INCH = 500 FPS.

SCHEMATIC DRAWING OF THE JET PUMPS

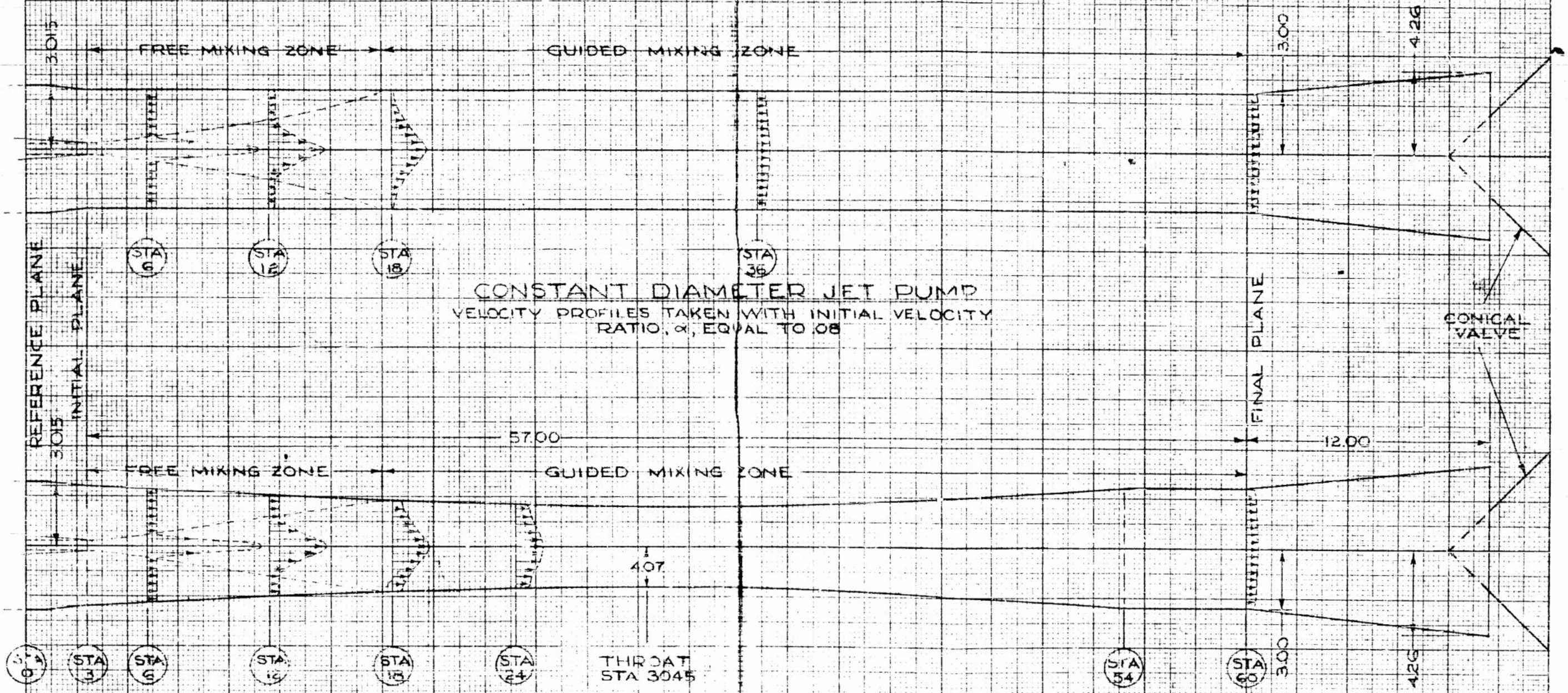

CONSTANT DIAMETER JET PUMP
VELOCITY PROFILES TAKEN WITH INITIAL VELOCITY RATIO, α, EQUAL TO .08

CONSTANT PRESSURE JET PUMP
VELOCITY PROFILES TAKEN WITH INITIAL VELOCITY RATIO, α, EQUAL TO .069

FIGURE 5

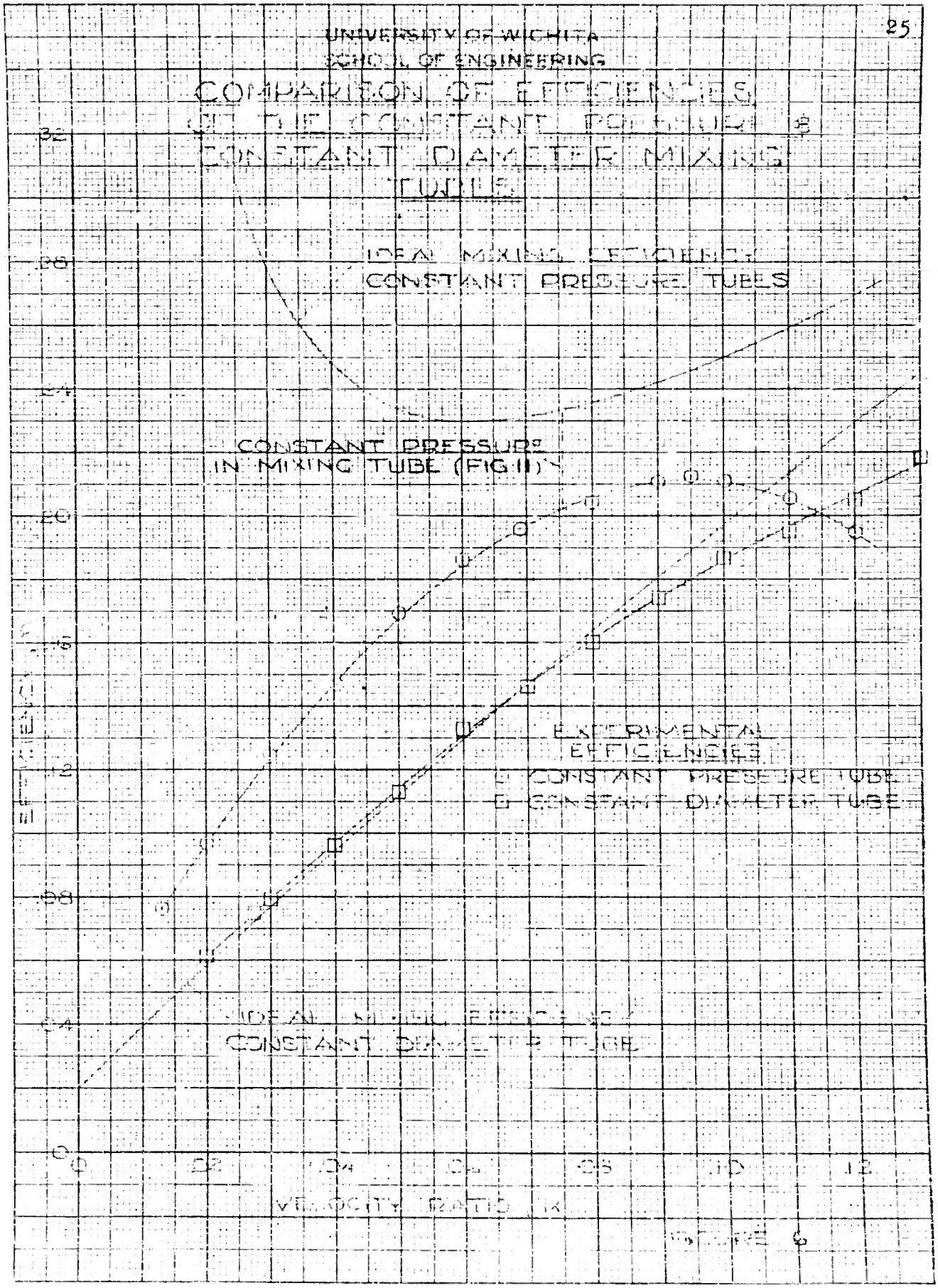
UNIVERSITY OF WICHITA
SCHOOL OF ENGINEERING
COMPARISON OF EFFICIENCIES
OF THE CONSTANT PRESSURE &
CONSTANT DIAMETER MIXING
TUBES
IDEAL MIXING EFFICIENCY
CONSTANT PRESSURE TUBES
CONSTANT PRESSURE
IN MIXING TUBE (FIG II)
EXPERIMENTAL
EFFICIENCIES
CONSTANT PRESSURE TUBE
CONSTANT DIAMETER TUBE
IDEAL MIXING EFFICIENCY
CONSTANT DIAMETER TUBE
EFFICIENCY
VELOCITY RATIO
.98
.96
.94
.92
.90
.88
.86
.84
.82
.80
0
.2
.4
.6
.8
1.0
1.2

UNIVERSITY OF WICHITA
SCHOOL OF ENGINEERING

VARIATION OF MASS RATIO WITH VELOCITY RATIO

○ CONSTANT PRESSURE MIXING TUBE (DESIGN α = .065)
□ CONSTANT DIAMETER MIXING TUBE

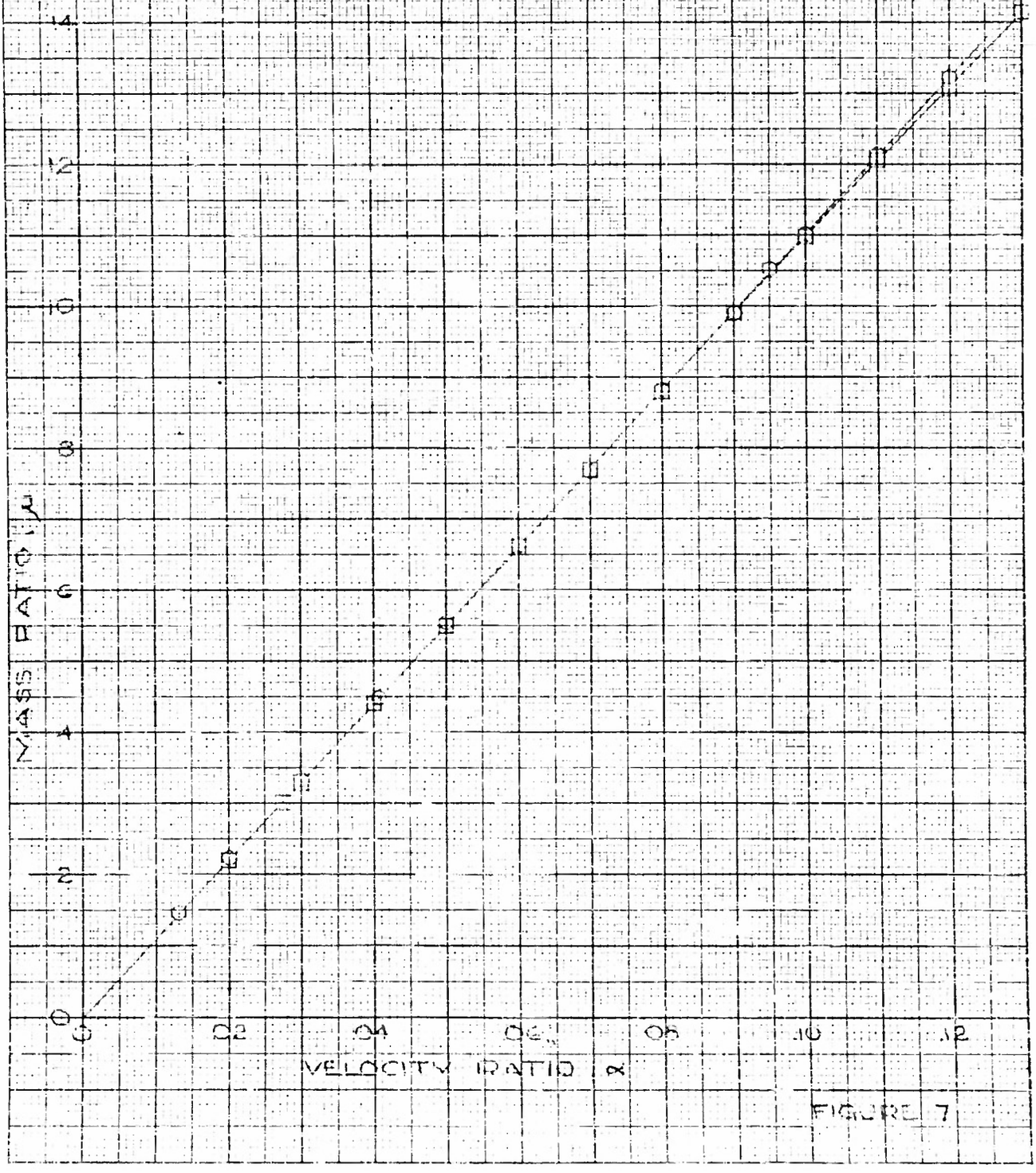

FIGURE 7

UNIVERSITY OF WICHITA
SCHOOL OF ENGINEERING

VARIATION OF TRANSMISSION COEFFICIENT WITH VELOCITY RATIO

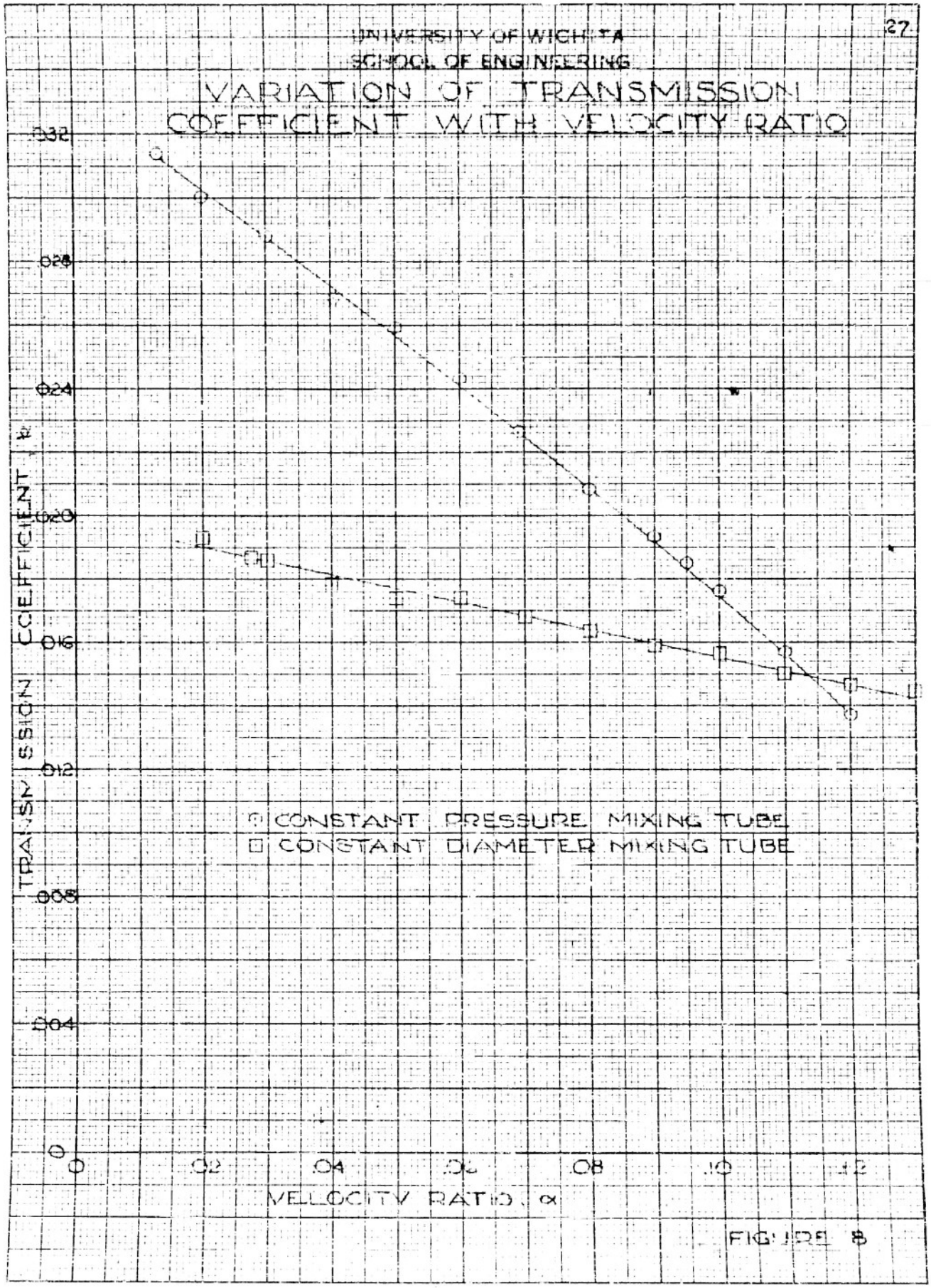

FIGURE 8

UNIVERSITY OF WICHITA
SCHOOL OF ENGINEERING
COMPARISON OF AXIAL STATIC PRESSURE DISTRIBUTIONS
CONSTANT DIAMETER & CONSTANT PRESSURE MIXING TUBES
D CONSTANT PRESSURE MIXING TUBE
□ CONSTANT DIAMETER MIXING TUBE
STATIC PRESSURE (GAUGE) PSIG
INITIAL PLANE
FINAL PLANE
TUNNEL STA (IN.)
10
20
30
40
50
60
2
4
6
8
10
12
14

FIGURE 9

UNIVERSITY OF WICHITA
SCHOOL OF ENGINEERING
COMPARISON OF AXIAL STATIC
PRESSURE DISTRIBUTION
CONSTANT DIAMETER & CONSTANT PRESSURE
MIXING TUBES
PUMP STAGE (IN.)
STATIC PRESSURE (GAUGE) K LBS/FT²
INLET PLANE
EXIT PLANE
10
20
30
40
50
60
2
4
6
8
10
12
14
16
18
20
22
10

UNIVERSITY OF WICHITA
SCHOOL OF ENGINEERING
AXIAL STATIC DISTRIBUTIONS
CONSTANT PRESSURE MIXING TUBE
DESIGN α = .069
STATIC PRESSURE GAUGE PSF
PUMP STATION (IN)
INT. AT PLANE
THROAT
STRAIGHT SECTION
FINAL PLANE
FIGURE 11

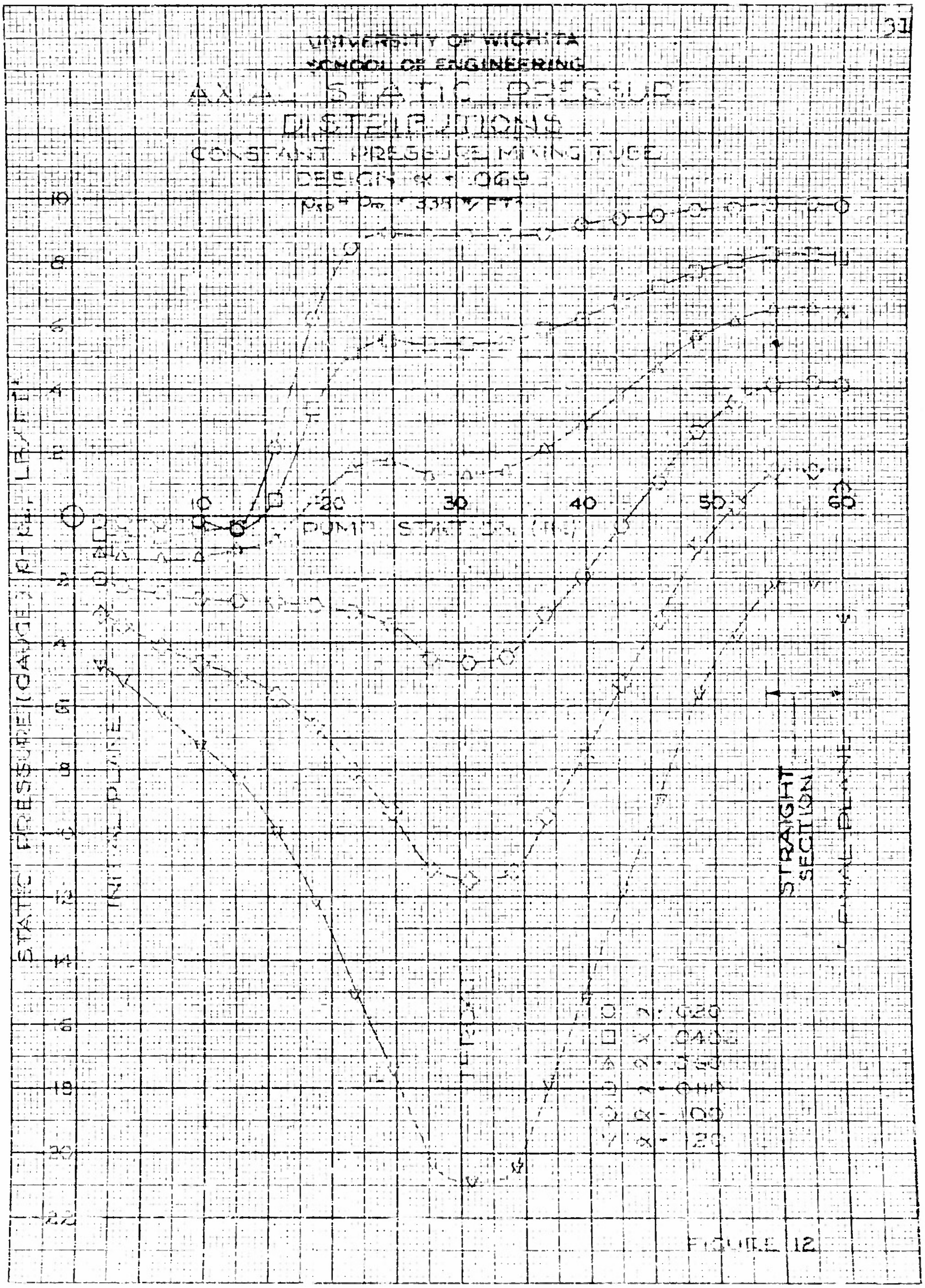
UNIVERSITY OF WICHITA
SCHOOL OF ENGINEERING
AXIAL STATIC PRESSURE
DISTRIBUTIONS
CONSTANT PRESSURE MIXING TUBE
STATIC PRESSURE (GAUGE)
PUMP STATION (IN.)
10
20
30
40
50
60
INITIAL PLANE
FINAL PLANE
STRAIGHT SECTION

FIGURE 12

UNIVERSITY OF WICHITA
SCHOOL OF ENGINEERING

AXIAL STATIC PRESSURE DISTRIBUTIONS

CONSTANT DIAMETER MIXING TUBE

$P_{mo} - P_s = 32.0$ #/FT²

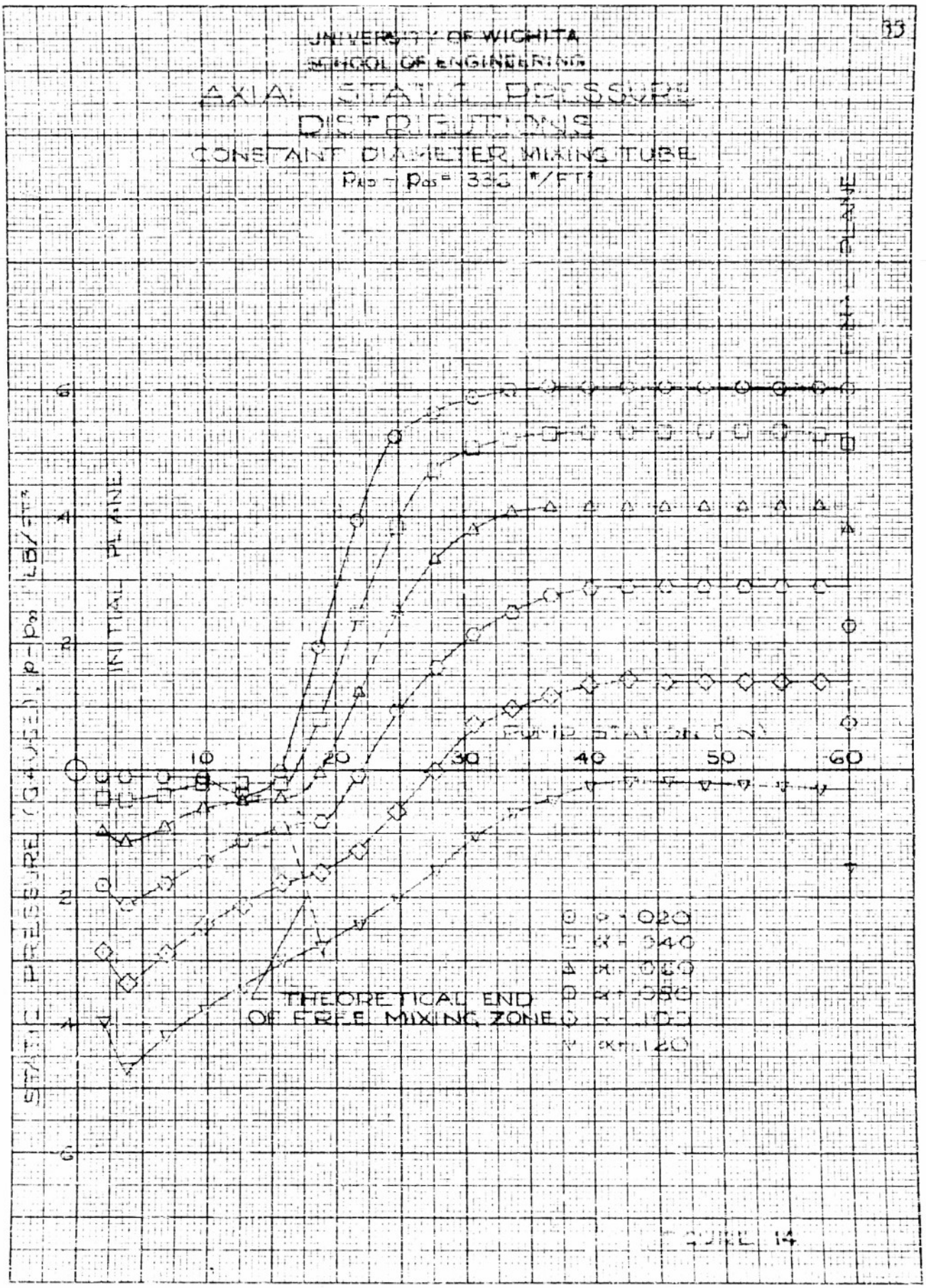
UNIVERSITY OF WICHITA
SCHOOL OF ENGINEERING
AXIAL STATIC PRESSURE
DISTRIBUTIONS
CONSTANT DIAMETER MIXING TUBE
$P_{AD} - P_{DS}$ = 335 #/FT²
STATIC PRESSURE (OUTSIDE) P-P_DS LB/FT²
INITIAL PLANE
EXIT PLANE
10
20
30
40
50
60
2
4
6
THEORETICAL END
OF FREE MIXING ZONE
R = 1.020
R = 1.040
R = 1.060
R = 1.080
R = 1.120

FIGURE 14

UNIVERSITY OF WICHITA
SCHOOL OF ENGINEERING

SIMILARITY OF STATIC-PRESSURE DISTRIBUTION IN GUIDED MIXING ZONE

CYLINDRICAL MIXING TUBE

FIGURE 15

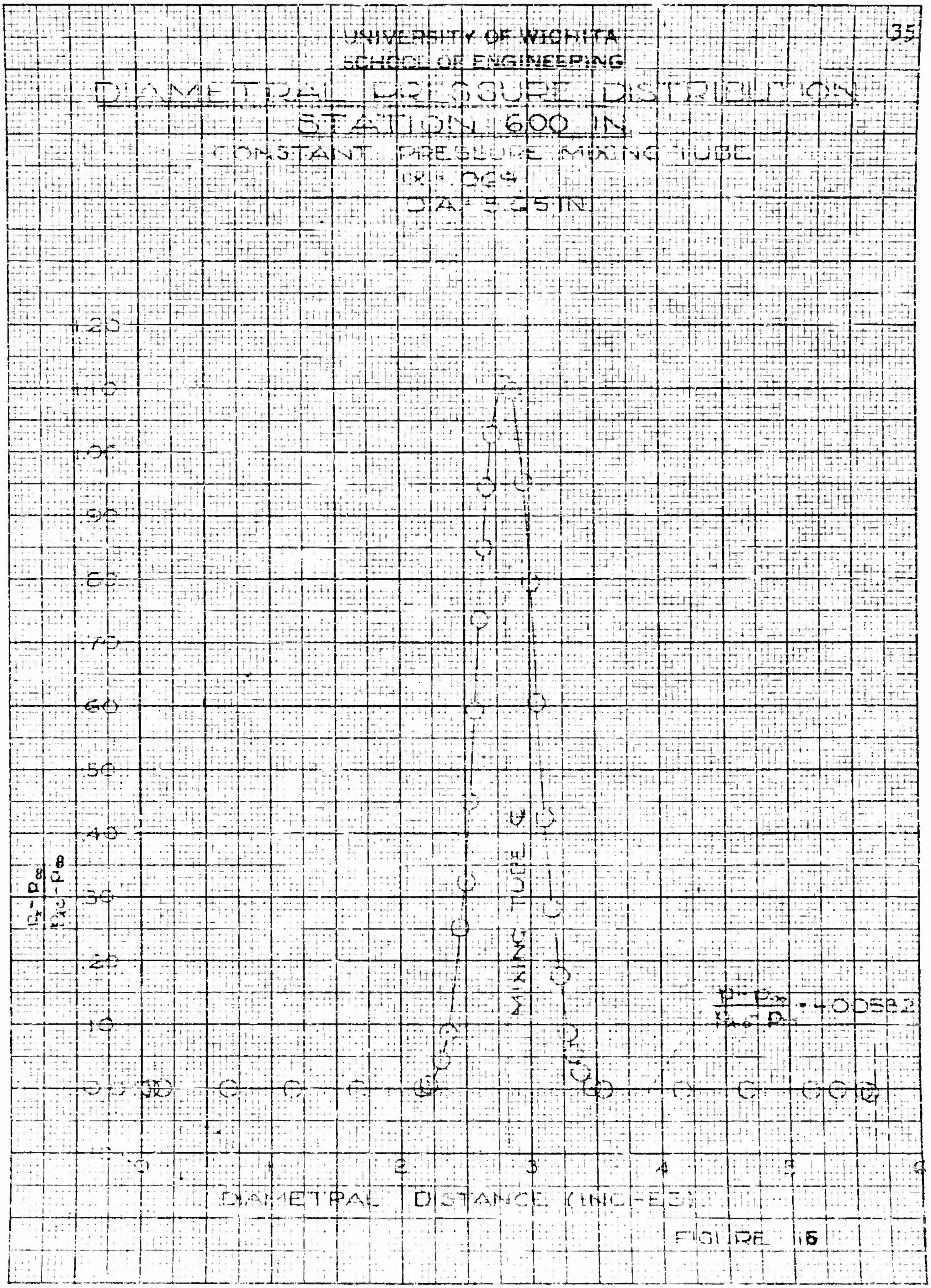
UNIVERSITY OF WICHITA
SCHOOL OF ENGINEERING
DIAMETRAL PRESSURE DISTRIBUTION
STATION 600 IN.
CONSTANT PRESSURE MIXING TUBE
MIXING TUBE
DIAMETRAL DISTANCE (INCHES)
FIGURE 15

UNIVERSITY OF WICHITA
SCHOOL OF ENGINEERING

DIAMETRAL PRESSURE DISTRIBUTION
STATION 1200 IN.

CONSTANT PRESSURE MIXING TUBE
4 HOLES
DIA = 5.03 IN

FIGURE 17

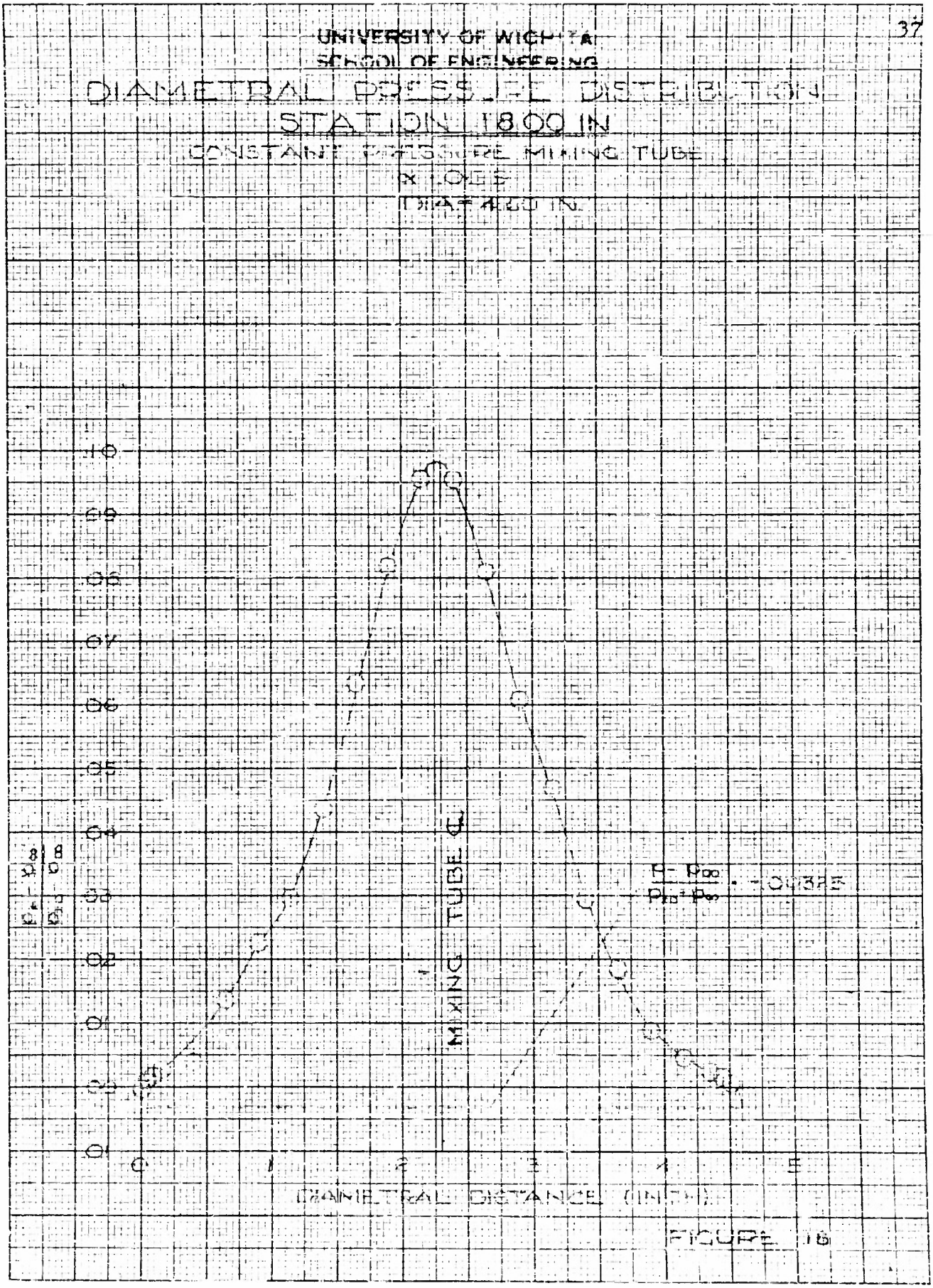
UNIVERSITY OF WICHITA
SCHOOL OF ENGINEERING
DIAMETRAL PRESSURE DISTRIBUTION
STATION 1800 IN
CONSTANT PRESSURE MIXING TUBE
& LOSS
DIAMETER IN.
MIXING TUBE
DIAMETRAL DISTANCE (INCH)
FIGURE 16

UNIVERSITY OF WICHITA
SCHOOL OF ENGINEERING
DIAMETRAL PRESSURE DISTRIBUTION
STATION 2400 IN.
CONSTANT PRESSURE MIXING TUBE
D = 0.59
DIA = 4.22 IN.
MIXING TUBE
DIAMETRAL DISTANCE (INCH)

FIGURE 19

UNIVERSITY OF WICHITA
SCHOOL OF ENGINEERING

DIAMETRAL PRESSURE DISTRIBUTION
STATION 60.00 IN.

CONSTANT PRESSURE MIXING TUBE
$\alpha = .069$
DIA = 6.00 IN.

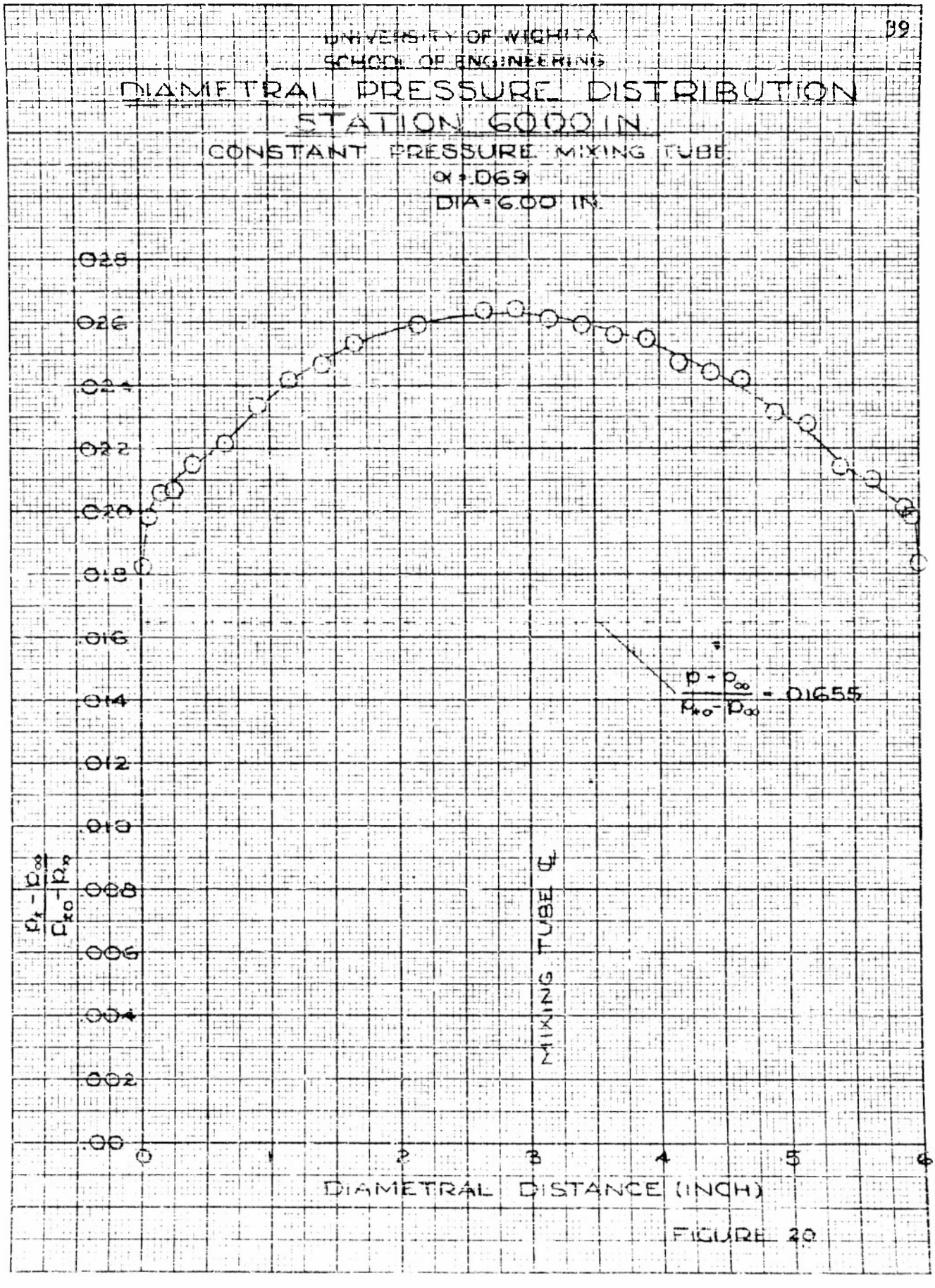

FIGURE 20

UNIVERSITY OF WICHITA
SCHOOL OF ENGINEERING

DIAMETRAL PRESSURE DISTRIBUTION
STATION 500 IN.
CONSTANT DIAMETER MIXING TUBE
X = 1.05
PLOT 6 IN

FIGURE 21

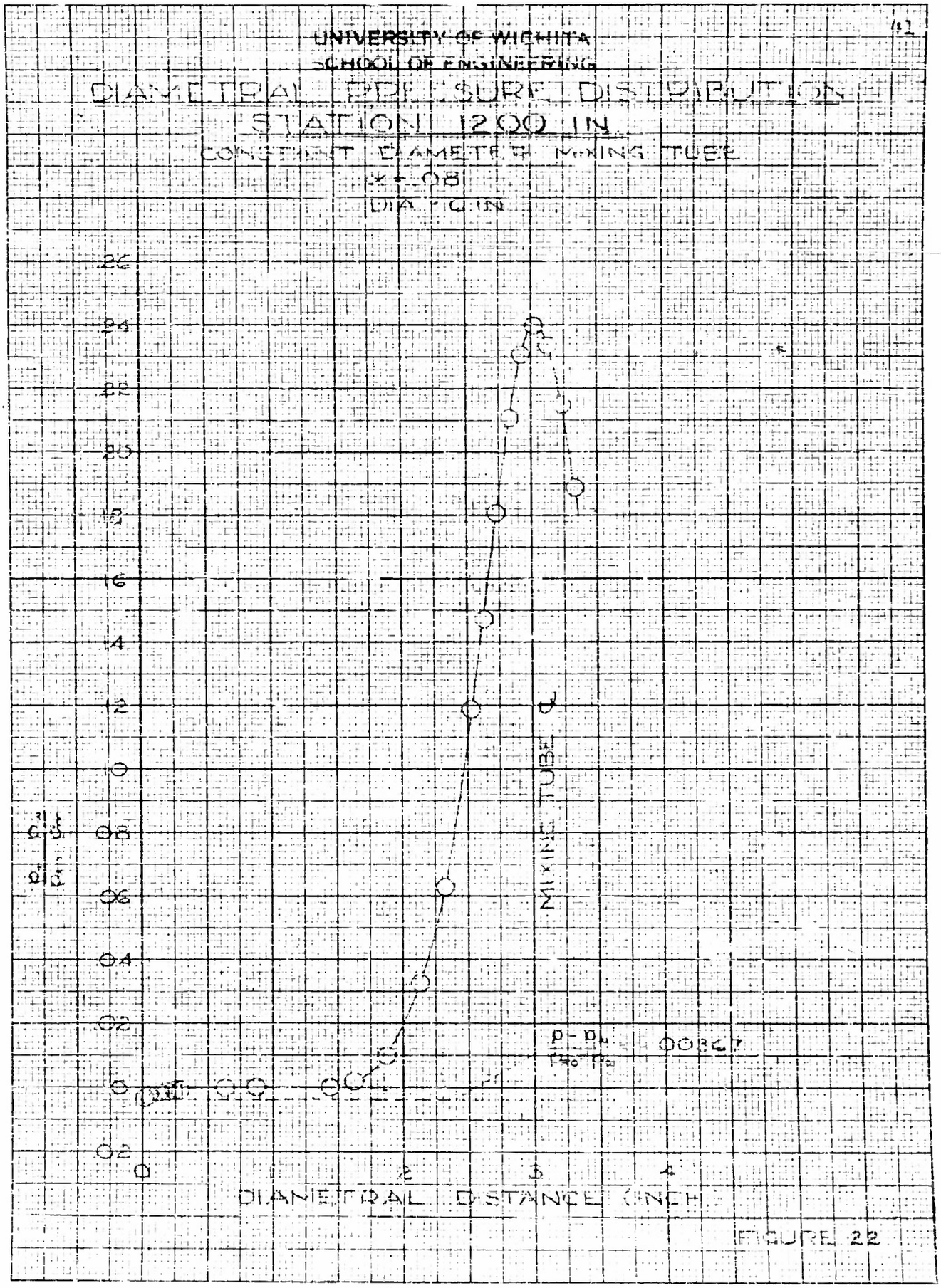
UNIVERSITY OF WICHITA
SCHOOL OF ENGINEERING
DIAMETRAL PRESSURE DISTRIBUTION
STATION 1200 IN
CONSTANT DIAMETER MIXING TUBE
X = .08
DIA 1.0 IN
MIXING TUBE
DIAMETRAL DISTANCE INCH
FIGURE 22

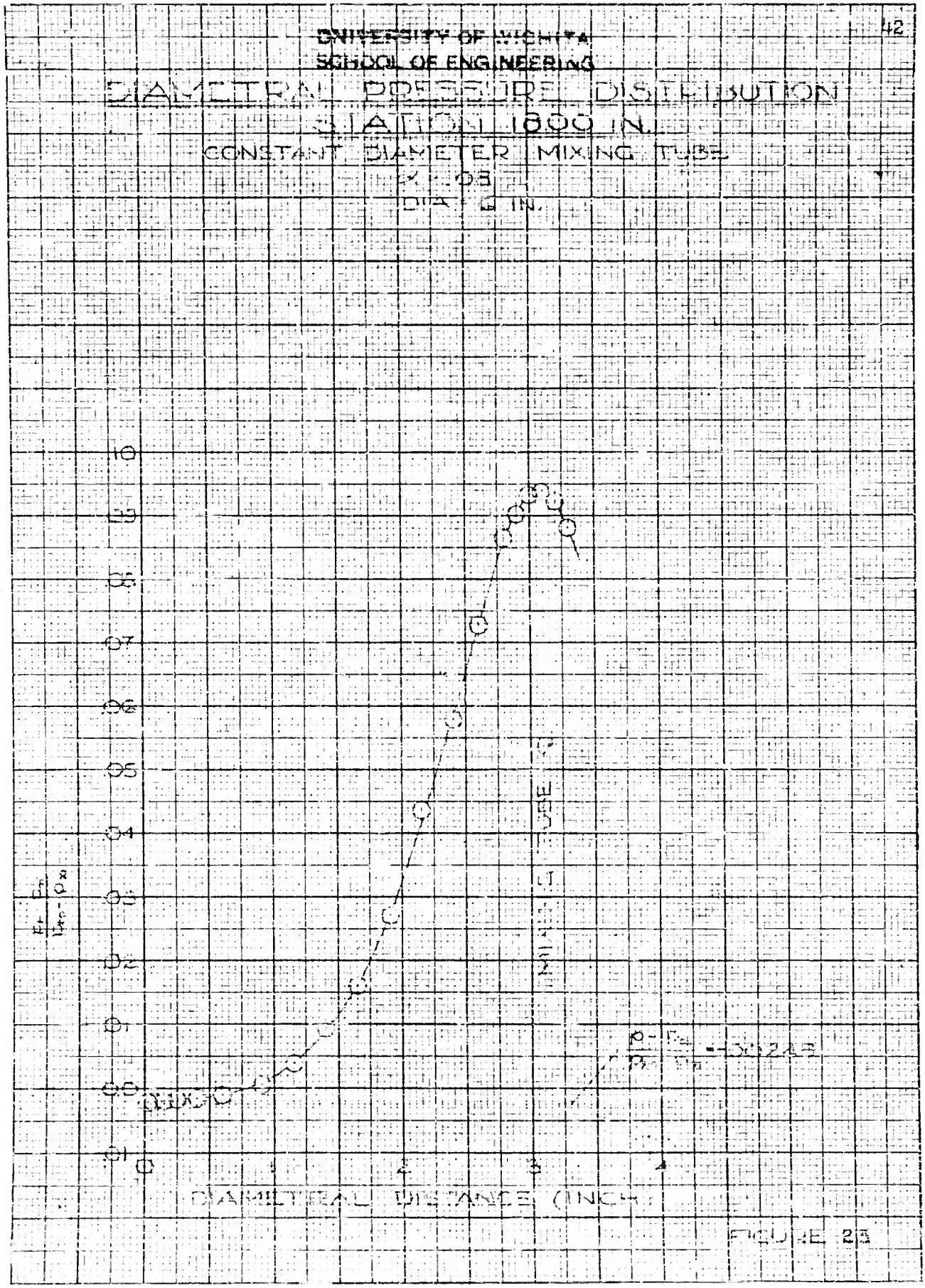
UNIVERSITY OF WICHITA
SCHOOL OF ENGINEERING
DIAMETRAL PRESSURE DISTRIBUTION
STATION 1800 IN.
CONSTANT DIAMETER MIXING TUBE
DIA = 6 IN.
DIAMETRAL DISTANCE (INCH)
FIGURE 23

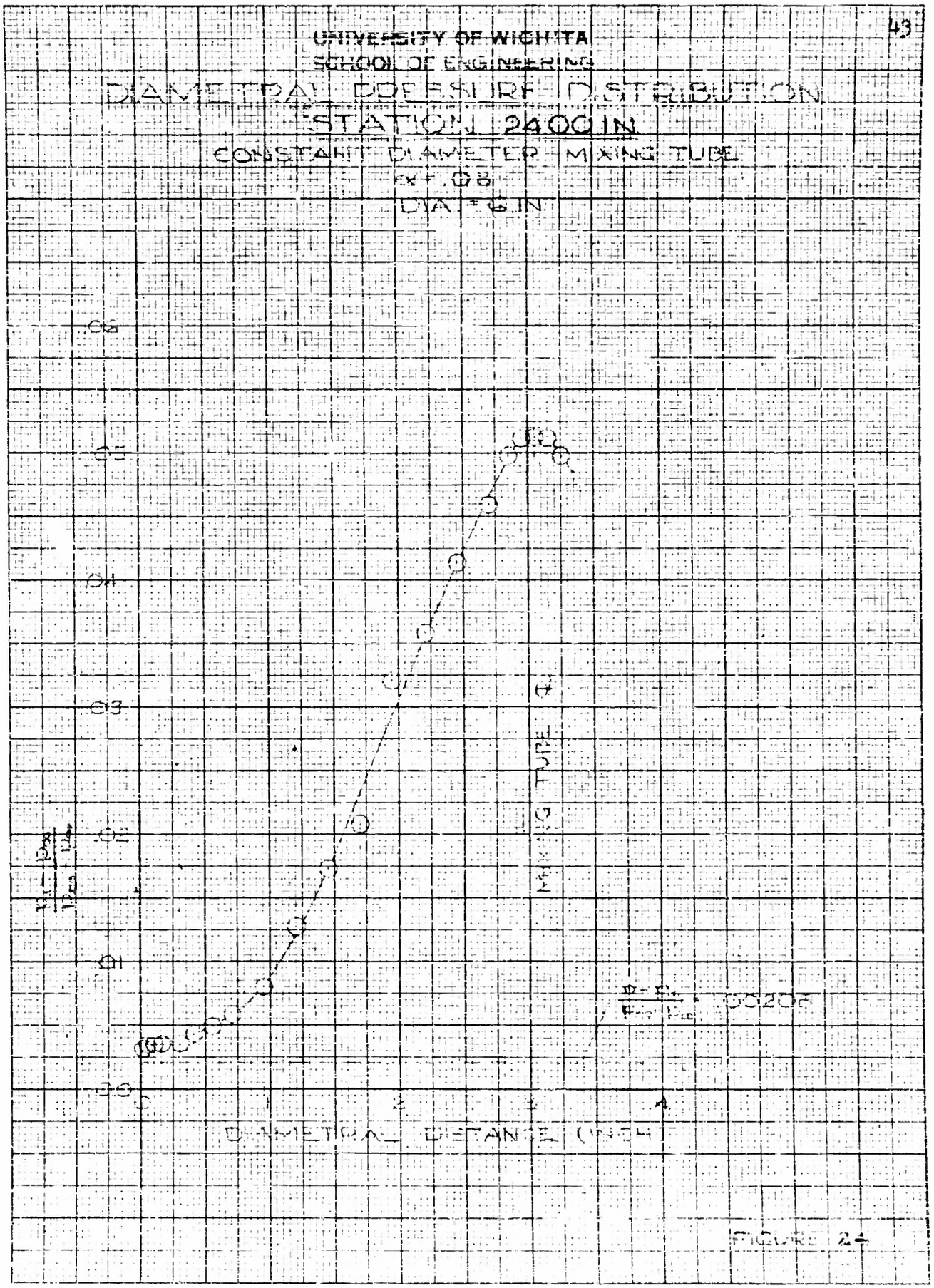
UNIVERSITY OF WICHITA
SCHOOL OF ENGINEERING
DIAMETRAL DOF PRESSURE DISTRIBUTION
STATION 2400 IN
CONSTANT DIAMETER MIXING TUBE
EXIT DIA = 6 IN
MIXING TUBE
DIAMETRAL DISTANCE (INCH)

FIGURE 24

UNIVERSITY OF WICHITA
SCHOOL OF ENGINEERING

DIAMETRAL PRESSURE DISTRIBUTION
STATION 3000 IN.
CONSTANT DIAMETER MIXING TUBE
R = 58
DA = 6 IN.

FIGURE 25

UNIVERSITY OF WICHITA
SCHOOL OF ENGINEERING

DIAMETRAL PRESSURE DISTRIBUTION
STATION 3600 IN

CONSTANT DIAMETER MIXING TUBE

M + 0A

DATED IN.

FIGURE 25

KEUFFEL & ESSER CO. MADE IN U.S.A.
10 X 10 TO THE INCH
359-11

UNIVERSITY OF WICHITA
SCHOOL OF ENGINEERING

DIAMETRAL PRESSURE DISTRIBUTION

STATION 4.00 IN.

CONSTANT DIAMETER MIXING TUBE

$R = 1.08$

DIA. = 6 IN.

FIGURE 27

UNIVERSITY OF [illegible]
SCHOOL OF ENGINEERING

DIAMETRAL PRESSURE DISTRIBUTION
STATION 60.00 IN
CONSTANT DIAMETER MIXING TUBE
$C_x = .08$
DIA = 6.00 IN.

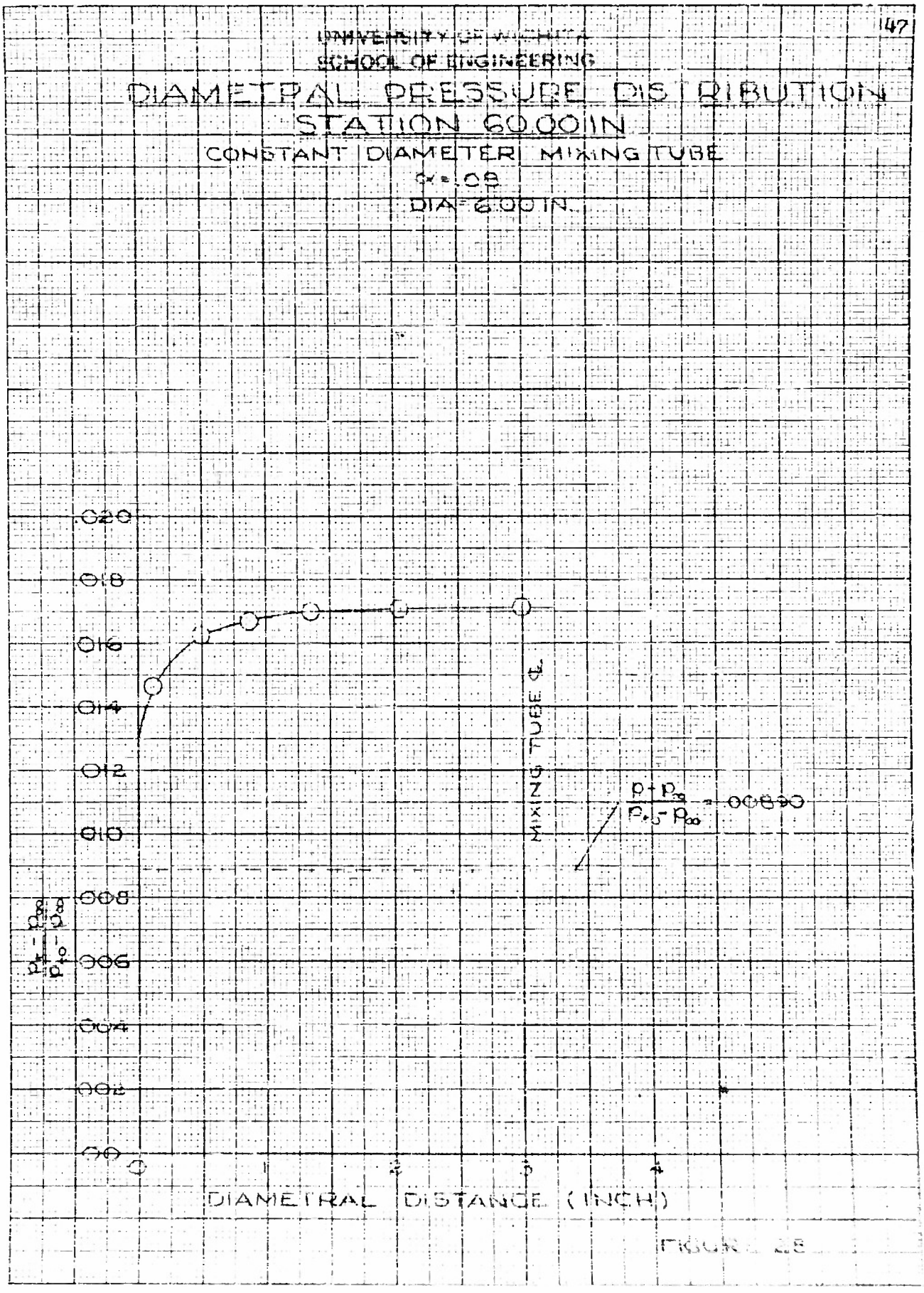

FIGURE 28

UNIVERSITY OF WICHITA
SCHOOL OF ENGINEERING

RADII OF HALF MAXIMUM EXCESS VELOCITY & RADII OF ZERO VEL

CONSTANT DIAMETER MIXING TUBE - 6" ∅

RADII OF HALF MAXIMUM EXCESS VELOCITY (EQUALS RAD. WHERE $\frac{V-V_{min}}{V_{max}-V_{min}} = \frac{1}{2}$ AT A SECTION)

RADII OF ZERO VELOCITY

MIXING TUBE WALL

REGION OF REVERSE FLOW

INITIAL PLANE

NOZZLE RAD. 295 IN

RADIAL DISTANCE (INCH)

JET PUMP STATION (INCHES)

0 4 8 12 16 20 24 28

FIGURE 25

KEUFFEL & ESSER CO. 10 X 10 TO THE INCH 1133

UNIVERSITY OF WICHITA
SCHOOL OF ENGINEERING

DIAMETRAL PRESSURE DISTRIBUTION

STATION 6.00 IN.

CONSTANT DIAMETER MIXING TUBE

[illegible]

DIA. 2.00 IN.

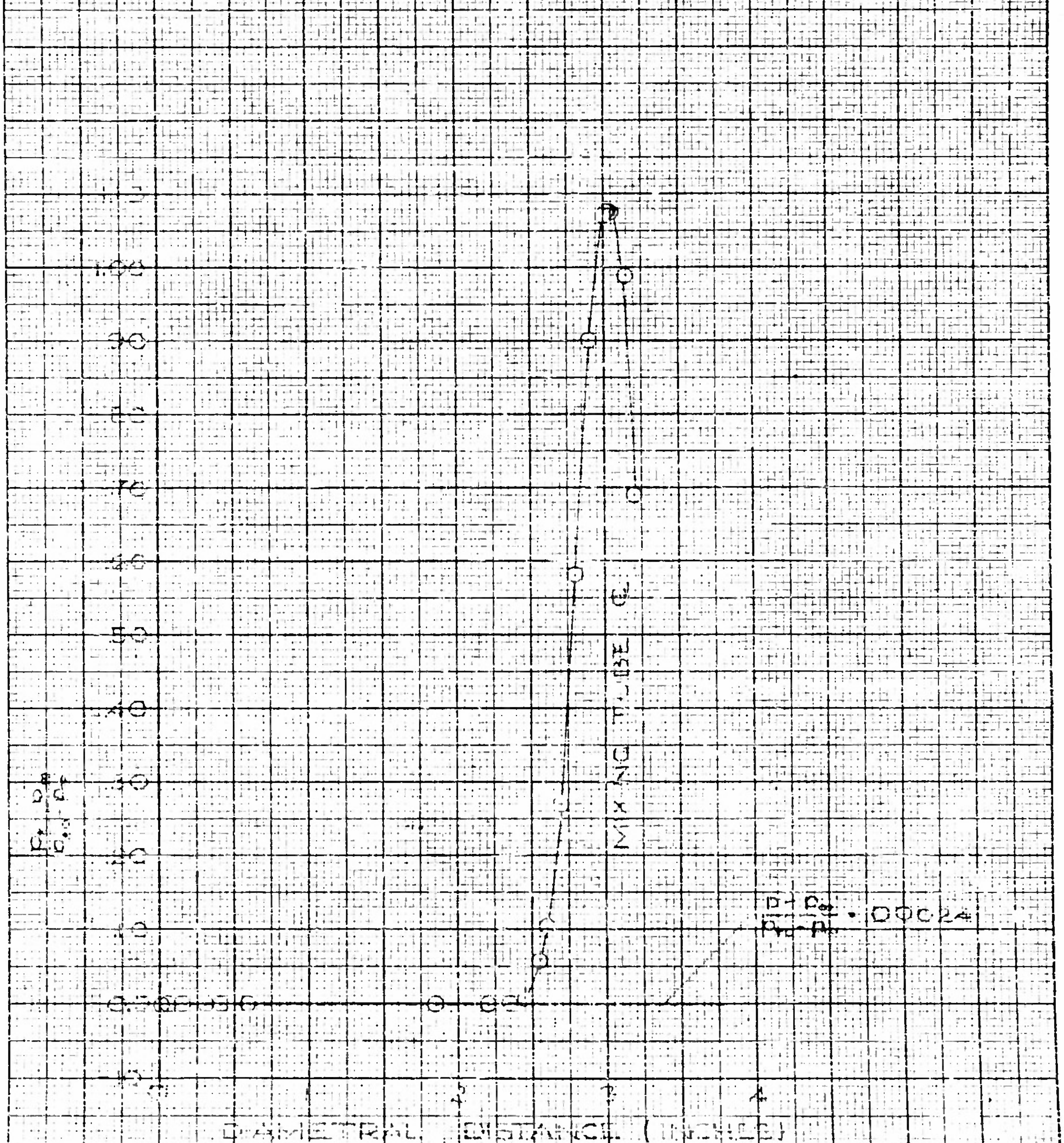

FIGURE 30

UNIVERSITY OF WICHITA
SCHOOL OF ENGINEERING

DIAMETRAL PRESSURE DISTRIBUTION
STATION 12.00 IN.

CONSTANT DIAMETER MIXING TUBE
$\beta = .02$
MACH 0.00

FIGURE 31

UNIVERSITY OF WICHITA
SCHOOL OF ENGINEERING
DIAMETRAL PRESSURE DISTRIBUTION
STATION 1800 IN
DIAMETRAL DISTANCE (INCHES)
FIGURE 38

UNIVERSITY OF WICHITA
SCHOOL OF ENGINEERING

DIAMETRAL PRESSURE DISTRIBUTION
STATION 24.00 IN.

CONSTANT DIAMETER MIXING TUBE
$\alpha = .02$
D.A. = 2.00 IN

REGION OF REVERSE FLOW

$\frac{P - P_4}{P_{x0} - P_4}$ = DIFF.

$\frac{P_1 - P_3}{P_2 - P_3}$

MIXING TUBE

DIAMETRAL DISTANCE (INCHES)

FIGURE 35

UNIVERSITY OF WICHITA
SCHOOL OF ENGINEERING

DIAMETRAL PRESSURE DISTRIBUTION
STATION 30.00 IN.

CONSTANT DIAMETER MIXING TUBE
α = .202
D = 6.00 IN.

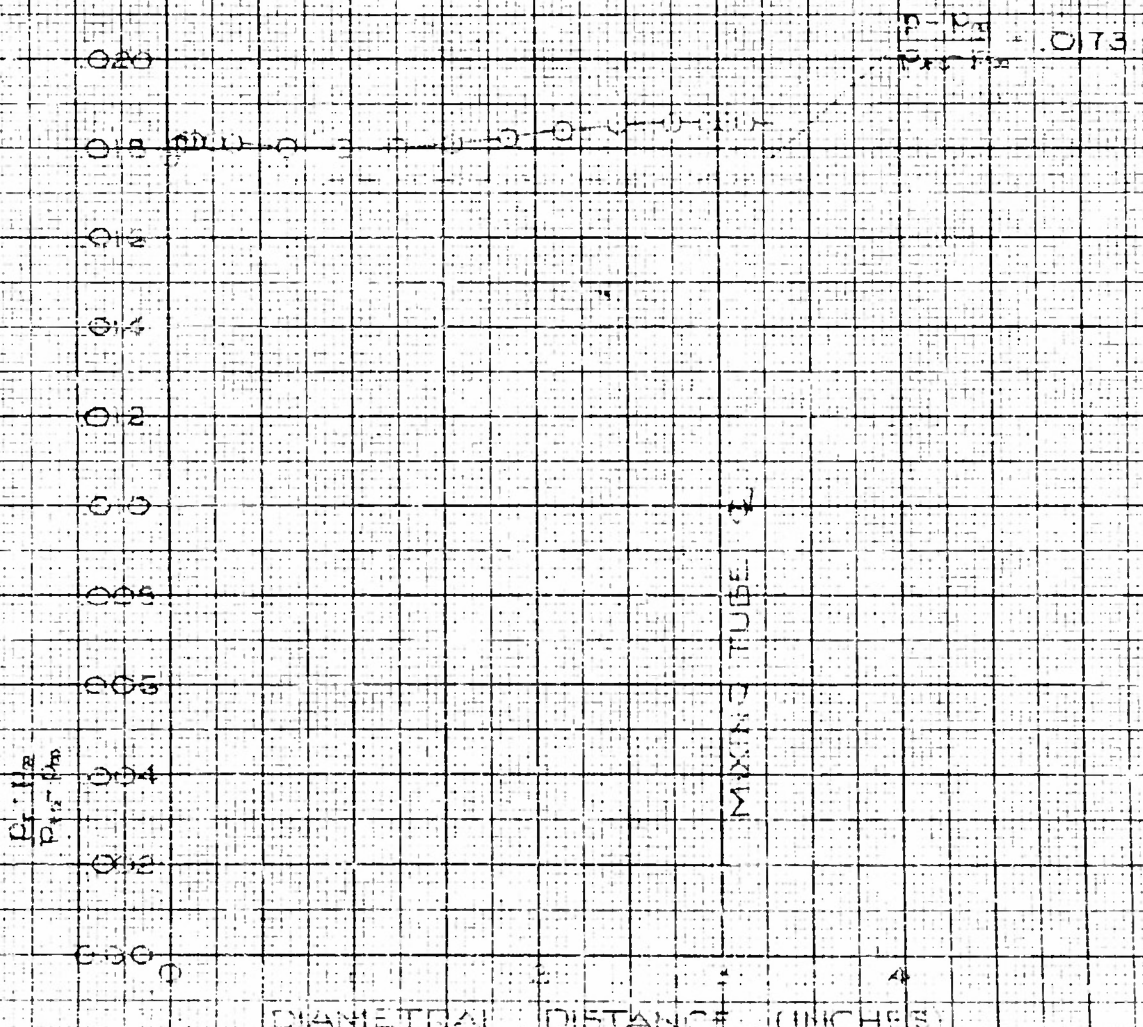

FIGURE 34

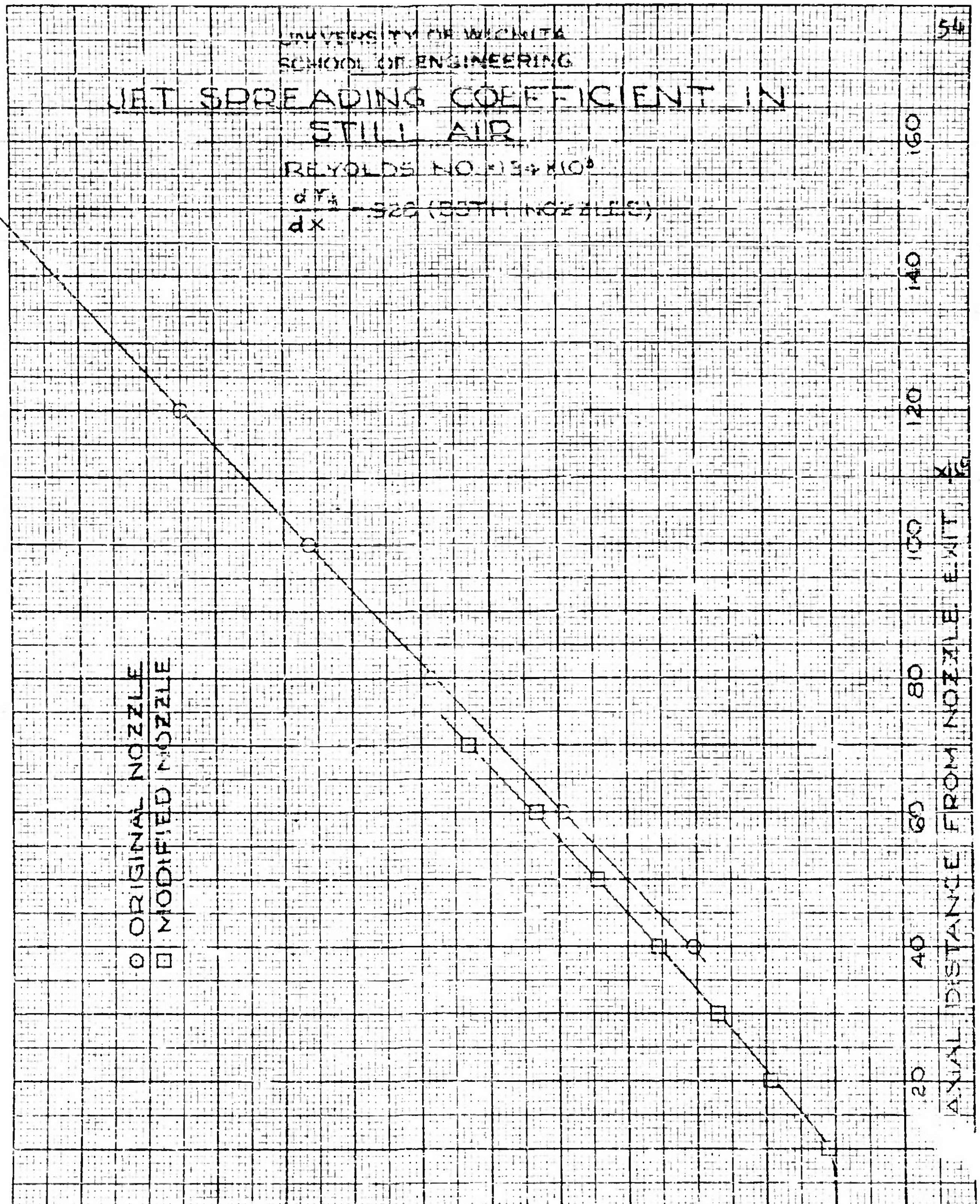

FIGURE 35

UNIVERSITY OF WICHITA
SCHOOL OF ENGINEERING
STATIC PRESSURE p*, AT
THE END OF THE FREE MIXING ZONE
CYLINDRICAL MIXING TUBE
EXPERIMENT
THEORY
TOTAL PRESSURE COEFFICIENT, Cp
A*/A2 = 2.552
FIGURE 36

UWER No. 147
University of Wichita, School of Engineering
AN EXPERIMENTAL COMPARISON OF CONSTANT-PRESSURE AND CONSTANT-DIAMETER JET PUMPS: H.E. Helmbold, G. Lussen and A.M. Heinrich. July 1954. 55 pp., diagrs., photos., 12 refs.

Two jet pumps, one of conventional constant-diameter design and the other of constant-pressure design (design initial-velocity ratio = 0.069), having identical jet-nozzle to mixing-tube area ratios and over-all dimensions were compared for initial velocity ratios from 0.01 to 0.13.

With a constant static pressure gradient in its free-mixing section (initial-velocity ratio = 0.0755), the constant-pressure jet-pump efficiency was 20.3 percent or 87.1 percent of the value theoretically predicted. This corresponded to a 31 percent improvement over the cylindrical jet pump efficiency which was 15.5 percent at the same initial velocity ratio ($\alpha = 0.0755$). With the cylindrical jet pump, experimental efficiencies slightly greater than predicted by theory were obtained with the ring vortex present ($\alpha < 0.0696$). Therefore the energy required to maintain a ring vortex was less than the energy conserved by mixing in the improved static pressure gradient which resulted from the vortex.

1.- Aerodynamics, Viscous Flow
2.- Jet Pump
I.- Helmbold, H.B.
II.- Lussen, G.
III.- Heinrich, A.M.
IV.- UWER No. 147

UWER No. 147
University of Wichita, School of Engineering
AN EXPERIMENTAL COMPARISON OF CONSTANT-PRESSURE AND CONSTANT-DIAMETER JET PUMPS: H.E. Helmbold, G. Lussen and A.M. Heinrich. July 1954. 55 pp., diagrs., photos., 12 refs.

Two jet pumps, one of conventional constant-diameter design and the other of constant-pressure design (design initial-velocity ratio = 0.069), having identical jet-nozzle to mixing-tube area ratios and over-all dimensions were compared for initial velocity ratios from 0.01 to 0.13.

With a constant static pressure gradient in its free-mixing section (initial-velocity ratio = 0.0755), the constant-pressure jet-pump efficiency was 20.3 percent or 87.1 percent of the value theoretically predicted. This corresponded to a 31 percent improvement over the cylindrical jet pump efficiency which was 15.5 percent at the same initial velocity ratio ($\alpha = 0.0755$). With the cylindrical jet pump, experimental efficiencies slightly greater than predicted by theory were obtained with the ring vortex present ($\alpha < 0.0696$). Therefore the energy required to maintain a ring vortex was less than the energy conserved by mixing in the improved static pressure gradient which resulted from the vortex.

1.- Aerodynamics, Viscous Flow
2.- Jet Pump
I.- Helmbold, H.B.
II.- Lussen, G.
III.- Heinrich, A.M.
IV.- UWER No. 147

UWER No. 147
University of Wichita, School of Engineering
AN EXPERIMENTAL COMPARISON OF CONSTANT-PRESSURE AND CONSTANT-DIAMETER JET PUMPS: H.E. Helmbold, G. Lussen and A.M. Heinrich. July 1954. 55 pp., diagrs., photos., 12 refs.

Two jet pumps, one of conventional constant-diameter design and the other of constant-pressure design (design initial-velocity ratio = 0.069), having identical jet-nozzle to mixing-tube area ratios and over-all dimensions were compared for initial velocity ratios from 0.01 to 0.13.

With a constant static pressure gradient in its free-mixing section (initial-velocity ratio = 0.0755), the constant-pressure jet-pump efficiency was 20.3 percent or 87.1 percent of the value theoretically predicted. This corresponded to a 31 percent improvement over the cylindrical jet pump efficiency which was 15.5 percent at the same initial velocity ratio ($\alpha = 0.0755$). With the cylindrical jet pump, experimental efficiencies slightly greater than predicted by theory were obtained with the ring vortex present ($\alpha < 0.0696$). Therefore the energy required to maintain a ring vortex was less than the energy conserved by mixing in the improved static pressure gradient which resulted from the vortex.

1.- Aerodynamics, Viscous Flow
2.- Jet Pump
I.- Helmbold, H.B.
II.- Lussen, G.
III.- Heinrich, A.M.
IV.- UWER No. 147

UWER No. 147
University of Wichita, School of Engineering
AN EXPERIMENTAL COMPARISON OF CONSTANT-PRESSURE AND CONSTANT-DIAMETER JET PUMPS: H.E. Helmbold, G. Lussen and A.M. Heinrich. July 1954. 55 pp., diagrs., photos., 12 refs.

Two jet pumps, one of conventional constant-diameter design and the other of constant-pressure design (design initial-velocity ratio = 0.069), having identical jet-nozzle to mixing-tube area ratios and over-all dimensions were compared for initial velocity ratios from 0.01 to 0.13.

With a constant static pressure gradient in its free-mixing section (initial-velocity ratio = 0.0755), the constant-pressure jet-pump efficiency was 20.3 percent or 87.1 percent of the value theoretically predicted. This corresponded to a 31 percent improvement over the cylindrical jet pump efficiency which was 15.5 percent at the same initial velocity ratio ($\alpha = 0.0755$). With the cylindrical jet pump, experimental efficiencies slightly greater than predicted by theory were obtained with the ring vortex present ($\alpha < 0.0696$). Therefore the energy required to maintain a ring vortex was less than the energy conserved by mixing in the improved static pressure gradient which resulted from the vortex.

1.- Aerodynamics, Viscous Flow
2.- Jet Pump
I.- Helmbold, H.B.
II.- Lussen, G.
III.- Heinrich, A.M.
IV.- UWER No. 147

Good agreement between theoretical and experimental values was obtained for free-mixing zone lengths and static pressures at the end of the free mixing zone for the cylindrical jet pump.

Good agreement between theoretical and experimental values was obtained for free-mixing zone lengths and static pressures at the end of the free mixing zone for the cylindrical jet pump.

Good agreement between theoretical and experimental values was obtained for free-mixing zone lengths and static pressures at the end of the free mixing zone for the cylindrical jet pump.

Good agreement between theoretical and experimental values was obtained for free-mixing zone lengths and static pressures at the end of the free mixing zone for the cylindrical jet pump.